ALTA Center
TECHNICAL REPORT

Doc.No : ENV001
Version : 1.0
Date : 31/12/2019

ALTA Center: Advanced LBT Turbulence and Atmosphere Center Report 12/2019

PI: Elena Masciadri
TEAM: Alessio Turchi, Elena Masciadri

INAF/Osservatorio Astrofisico di Arcetri
L.go Enrico Fermi 5
50125 Florence, Italy

ABSTRACT

ALTA Center is a project funded by the Large Binocular Telescope Observatory conceived to support science operations of LBT and LBTI. The main goal is to set-up a completely automatic system to forecast the most important atmospheric and astroclimatic parameters (seeing, isoplanatic angle, wavefront coherence time) relevant for the ground-based astronomical observations, particularly those supported by Adaptive Optics. The project started on 2015 and it has been conceived as a long term project and it is organised on a sequence of contracts of typically five years. The plan has been defined and agreed with the LBTO Director so to be able to supply the required informations on the atmospheric conditions necessary for the LBTO facilities operations, particularly those supported by the Adaptive Optics and the Interferometry.

The project has been warmly solicited by the LBTO Director, Christian Veillet as a piece of a more extended plan aiming to equip LBTO with a set of tools/instrumentations necessary to provide a complete monitoring and characterisation of the atmosphere of Mt.Graham, site of the LBT. The outputs of ALTA Center are supposed to be injected in the LBT Science Operation system designed to optimise the management of the LBT observations [1]. The first contract of ALTA has been conceived to cover a five years activity in the period 2015-2019.

At present time ALTA Center is one of the very few centers existent in the astronomical context at a worldwide scale that is able to predict all the key atmospherical and astroclimatic parameters relevant for the ground-based astronomy. It is at our knowledge the first and unique center that is able to provide forecasts at short time scales (i.e. a few hours) with such accuracies (see Section 7).

It is important to mention that ALTA Center is in continuous evolution. A few functionalities of ALTA could not yet been validated because of a lack of presence of dedicated monitors in situ that are however supposed to be implemented in the next future (for example a MASS - Multi Aperture Scintillation Sensor). This will be included in a forthcoming contract.

Contents

1 Acronimes

LBT: Large Binocular Telescope

LBTI: Large Binocular Telescope Interferometer

LBTO: Large Binocular Telescope Observatory

ECMWF: European Center for Medium range Weather Forecasts

INAF-OAA: Istituto Nazionale di Astrofisica / Osservatorio Astrofisico di Arcetri

CED: Elaboration Data Center

GCM: General Circulation Model

OT: Optical Turbulence

SCIDAR: SCIntillation Detection and Range

GS: Generalised SCIDAR

IFS: Integrated Forecast System (of ECMWF)

NOAA: National Oceanic Atmospheric Administration

NCAR: National Center for Atmospheric Research

GFS: Global Forecast System (of NOAA)

2 Introduction

Goal of this report is to describe the state of the art of the contract ENV001 named Advanced LBT Turbulence and Atmosphere Center (ALTA Center). An agreement has been signed between the Large Binocular telescope Observatory (LBTO) and INAF-Osservatorio Astrofisico di Arcetri (OAA) through a Memorandum of Understanding on 2014 October. The contract has been conceived to last five years and to be renovated with new budget according to new objectives (to be discussed and agreed with LBTO) on a time scale of five years. The first contract started on 1st January 2015 and lasted up to 31th December 2019.

The main goals of the ALTA Center project for the [2015-2019] period are:

- to conceive and develop for the LBT and LBTI an automatic and operational system for the forecast of the optical turbulence (OT) and the atmospheric parameters relevant for the ground-based astronomy supported by the Adaptive Optics (AO);

- to calibrate the model for those parameters for which is necessary and to validate the model with measurements used as a a reference. With OT we mean C_N^2 profiles and integrated astroclimatic parameters. The most relevant astroclimatic parameters treated in this contract have been: the seeing (ε), the isoplanatic angle (θ_0) and the wavefront coherence time (τ_0). The atmospheric parameters treated in this study are: the absolute temperature (T), the wind speed (WS) and direction (WD), the relative humidity (RH) and the precipitable water vapour (PWV)[1].

The contract is organised in four different phases scheduled through four different milestones (see MoU) that we report here:

Milestone 1: Automation of the system, acquisition and installation, configuration of the hardware/software, web page set-up (first year)

Milestone 2: Development and deployment of the atmospheric parameters prediction with corresponding data access capabilities from LBTO

Milestone 3: Development and deployment of the optical turbulence prediction with corresponding data access capabilities from LBTO

Milestone 4: Automated meta-data archival

The MoU contained in Annex a detailed list of deliverables mainly for Phase 2 and Phase 3 (i.e. for Milestone 2 and Milestone 3).

In this report we summarise the outputs of the study. We highlight the fact that the study has been organised with monthly meeting with the LBTO counterpart (Veillet, Christou) in which the progresses of the project were discussed. In the FOSWiKi ($http://aowiki.arcetri.astro.it/ALTA/WebHome$) repository have been posted the contents of the meetings mainly summarized in *pptx (or *pdf) presentations.

This project lead to the publication of three papers in Peer-Reviewed Journals and a number of papers on Conference Proceedings in which the on-going progresses of the study have been presented (see Section 8). All along the report, we will refer the reader to the respective papers where it is necessary.

[1] The PWV was not originally included in the contract

3 Milestone 1: Automation of the system, acquisition and installation, configuration of the hardware/software, web page set-up (one year)

The core of ALTA Center system is based on the Meso-Nh atmospherical model and the Astro-Meso-NH code. The Meso-Nh model is a mesoscale model, developped by the Centre Nationale des Recherches Meteorologiques (CNRM) and Laboratoire d'Aerologie (LA) in Toulouse (France) [2, 3]. It is one among the most advanced atmospherical mesoscale models available at present mainly used by the French community[2]. The Astro-Meso-Nh code has been conceived to forecast the optical turbulence and the astroclimatic parameters. It was originally developed by Elena Masciadri a couple of decades ago [4, 5] and since there has been in continuous development by the author. More recently it is managed by the Optical Turbulence team in Arcetri.

Both codes (Meso-Nh and Astro-Meso-Nh) have been conceived for research purposes, so they don't include automatic procedures for configuration and operational forecasts on a daily basis and without manual intervention.
For this reason, the first step of the ALTA project was the development of a code conceived to automate all the different steps permitting to achieve the mesoscale atmospheric forecast and ensure a smooth operational environment to support daily forecasts with a robust procedure.

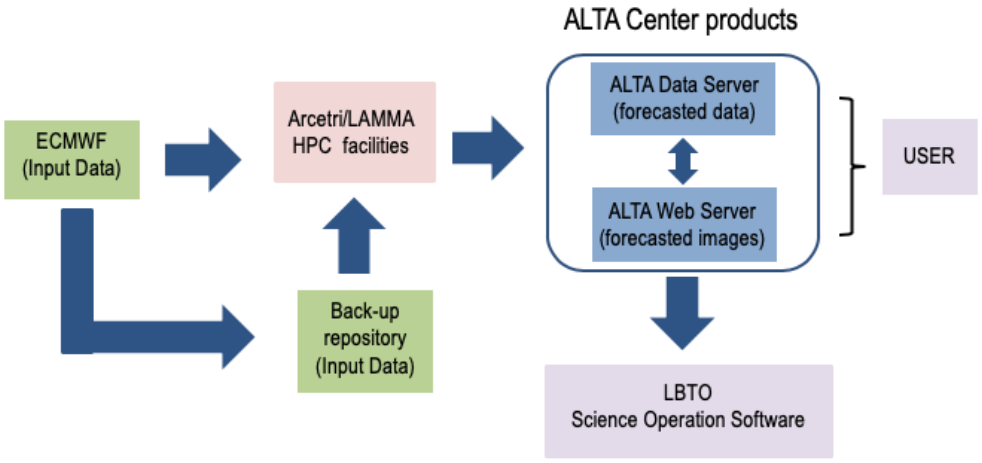

Figure 1: Flowchart of the automatic forecast scheme.

In Fig.1 is shown the general scheme showing the interconnection between the ALTA Center, the sources of initialisation and the outputs (users and the LBTO Science Operational Software). The boxes related to inputs are indicated in green, the boxes related to computation phase are indicated in pink, the boxes related to deployment and display phase are indicated in blue and the boxes related to the outputs are indicated in violet.

In Fig.2 is shown the detailed sequence of actions that are part of the automatic procedure that leads to the production of the forecast products.

[2]The model running actually on the national French country daily at 1 km of resolution contains the physics of Meso-Nh. We mention this fact just to highlight the fact that the physics of Meso-Nh is among the best we can access at present. Weather Research and Forecasting model (WRF) is another model of similar typology. We cite this mode as this has a large user community and it is more familiar by the scientific community.

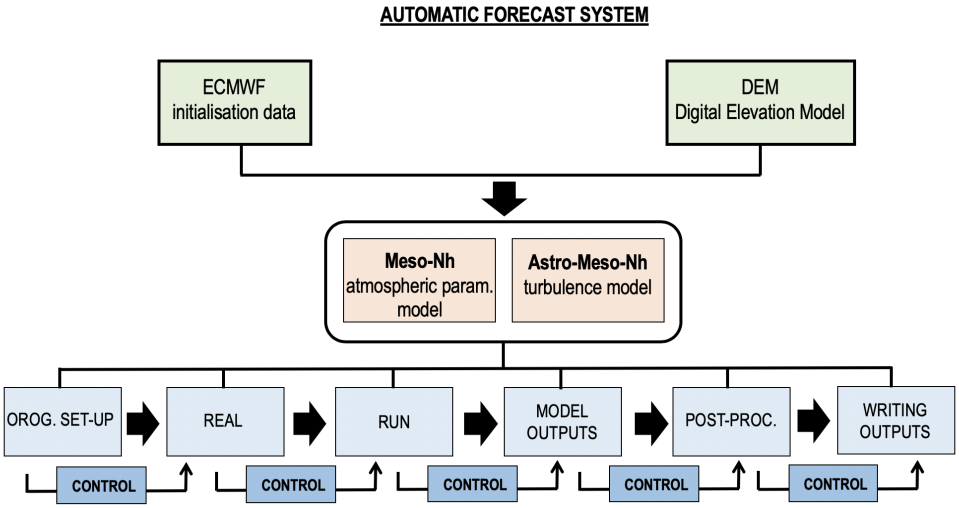

Figure 2: Schematic view of the automatic forecast system

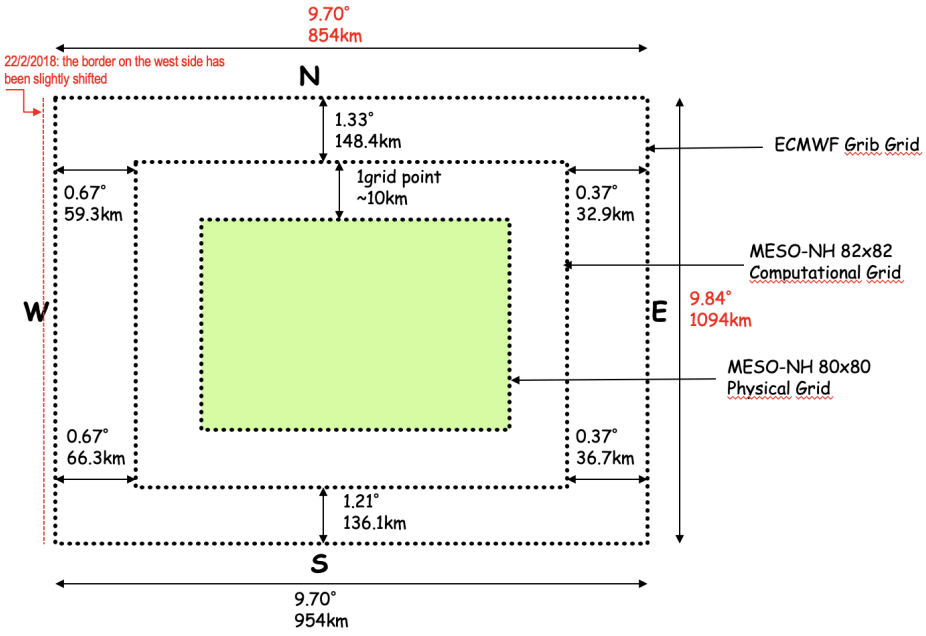

Figure 3: Borders of the outer Meso-NH simulation domain with respect to the grid-size of the ECMWF GCM.

The ALTA system automates all the Meso-NH operations. It first retrieves from the ECMWF initial grib files, containing the atmospheric state at large spatial scale obtained from the ECMWF Global Circulation Model, the relevant atmospheric data to initialise the mesoscale simulations. It generates the orography from the high-resolution Digital Elevation Model (DEM) and integrates in the orography all the cover data (terrain type, water mask, etc...). The orography is linked then to the atmospherical model. The geometry of the atmospheric model is obtained by defining the horizontal and vertical computational grid. The initialisation data are integrated onto the atmospheric model grid by adapting it to the orography. The mesoscale simulation operates in a grid-nesting configuration, with multiple simulation domains having progressively higher horizontal resolution 'nested' one into each other and extended on progressively smaller surfaces. In Fig.3 we report the

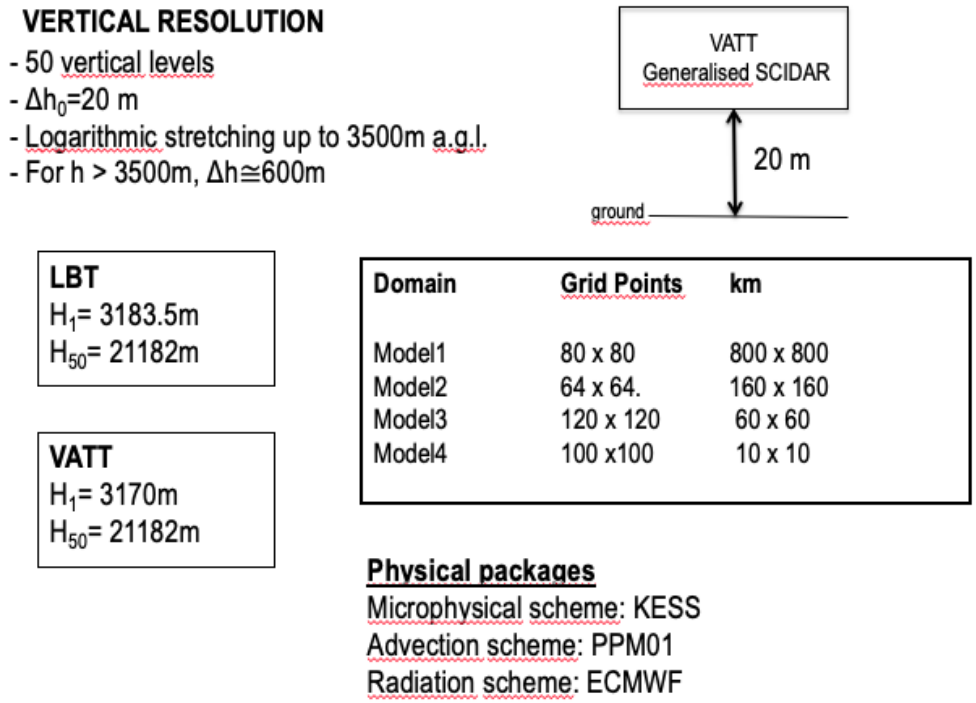

Figure 4: Model configuration: horizontal and vertical resolution; grid-nesting i.e. list of each nested simulation domains.

geographical limits of the retrieved initialisation data and the outer Meso-NH domain (800 km x 800 km).

We refer the reader to Turchi et al. 2017 [7] for a complete and detailed description of the configuration chosen for the grid-nesting of ALTA that consists on 4 domains.

Fig.4 summarises the main important elements such as the extension of the model domains, the horizontal and vertical grid distribution and the list of the main physical packages. Fig.5 shows the orographic maps of the four domains.

The forecast of all astroclimatic and atmospheric parameters, except wind speed, needs a horizontal resolution of the innermost domain equal to 500 m. That means that a 3 domains grid-nesting configuration is sufficient to provide the required forecasted parameters, while to correctly reconstruct the strong wind speed at ground level the model needs a horizontal resolution of the innermost domain equal to 100 m (i.e. a 4 domains configuration)[3]. More precisely, it has has been proved (see Turchi et al. 2017 [7] for more details) that the wind speed close to the surface is underestimated when the WS is strong. We therefore first identify a threshold (8.5 ms^{-1}) over which this effect appears evident and then we replace the wind speed reconstructed with the resolution of 100 m to that obtained with a 3 domains configuration and a resolution of 500 m. The vertical grid has a first grid point equal to 20 m. The choice has been taken for two reasons:
(1) 20 m above the ground (a.g.l.) is the height at which the Generalised SCIDAR (GS) is located. The GS run indeed at the focus of the VATT. Measurements we used to calibrate the model belong to past site testing campaign (43 nights - [8]);
(2) 20 m is more or less the height of trees all around the telescope. Preliminary tests revealed that the trees produce a slow down effect on the atmospheric flow. It is therefore useless to study the atmospheric flow below this height as it is not representative. The automatic procedures takes care to generate the computational grid

[3]Of course the expression "it is required" means that we select, in each context, the optimal trade-off between the computational resources and the suitable performances

for each nested domain up to the needed horizontal resolution.

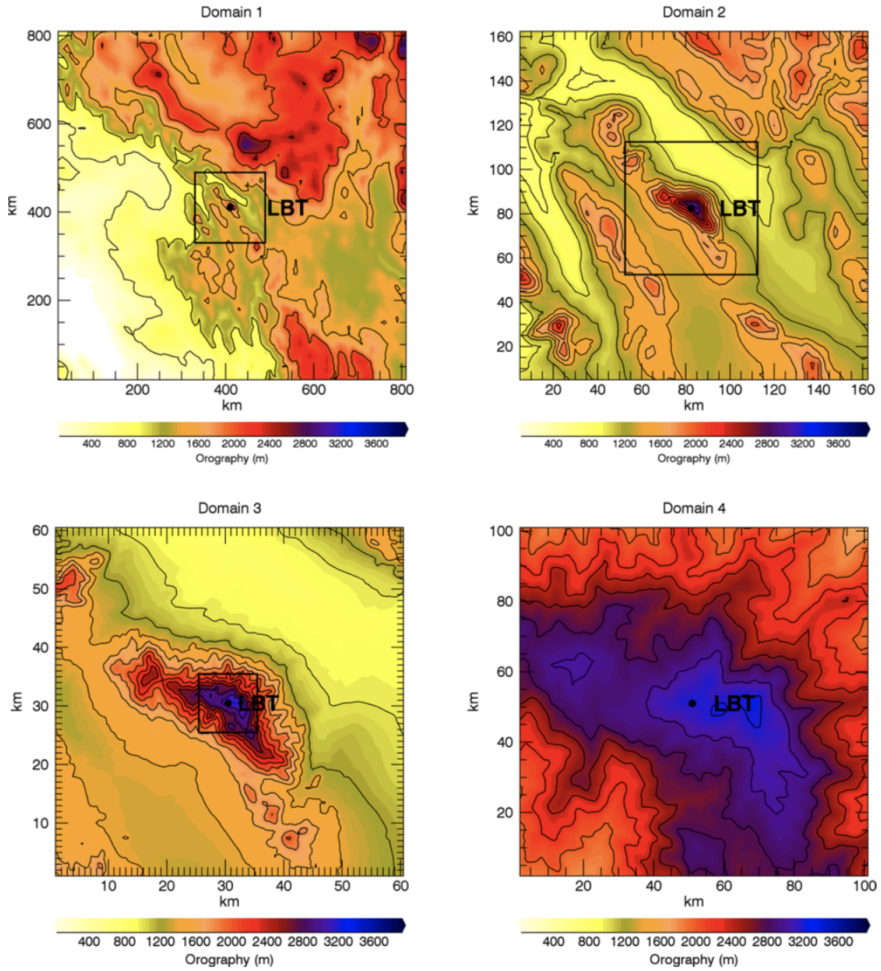

Figure 5: Horizontal maps of model nested domains, from the outer to the innermost domain, as reported in Fig.4. The black dot in the center of each domain corresponds to the position of LBT, while the colour scale represents the orography elevation.

After the computational grid definitions, the automation procedures automatically configures the Meso-NH simulations. The system runs consecutively a simulation on 3 domains (up to 500 m horizontal resolution) for the forecast of all astroclimatic and atmospheric parameters. In cases of strong wind speeds at ground, the system runs also a fourth domains simulation (up to 100 m horizontal resolution) to improve the reconstruction of the forecasted wind speed close to the surface. During the simulation the automatic system takes care of handling the exceptions, ensures the reliability of the forecast and chose the configuration that we verified to be the optimal one.

When the simulation is completed the automatic procedures performs the post-processing phase, in which all derived parameters (e.g. seeing ε, τ_0, precipitable water vapour (PWV), etc...) are computed. This phase is computationally intense because all the horizontal maps are extracted from the produced outputs (3D maps), so the automatic system optimises the whole phase to efficiently use the available hardware resources and ensures the timely delivery of the outputs. After the computation of the outputs the ALTA system automatically produces the graphic outputs, displays the outputs on the web-page (to be described later on) and delivers the

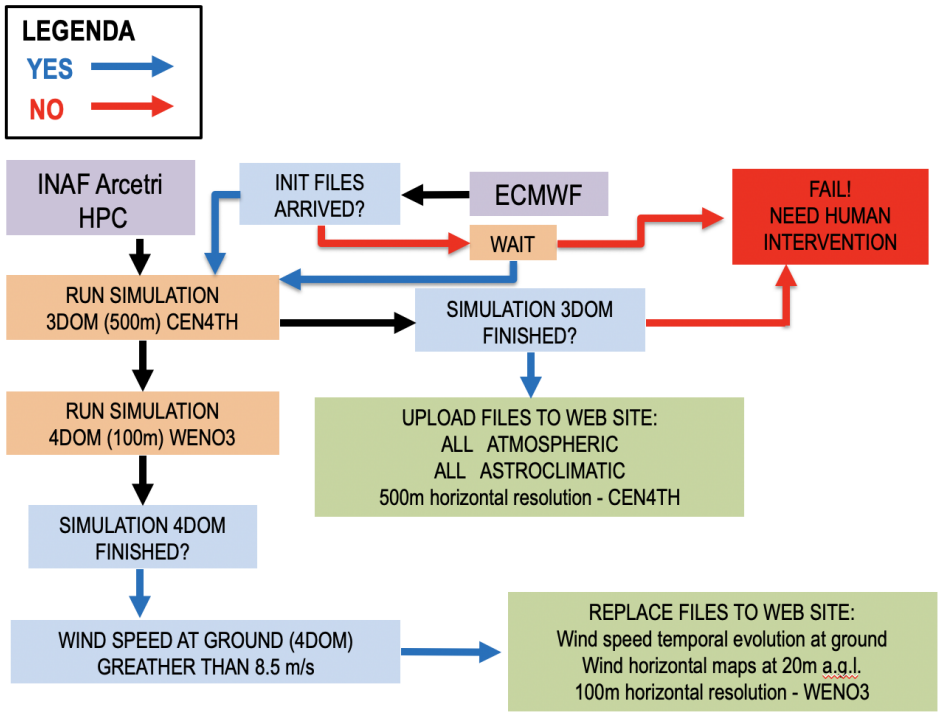

Figure 6: Decisional scheme supporting the automatic forecast procedure

ascii outputs for integration on the LBT Science Operation Software (see Fig.1). The ALTA automatic system is taking care of the error handling and is optimised to ensure that the LBT telescope can access a reliable forecast under most circumstances, reducing the need of human intervention to restore the system operations. In Fig.6 is shown the decisional scheme with respect to model failures.

Once the simulation is completed the raw outputs of the simulations (raw data) pass to the post-processing phase. At this stage the automatic procedure performs a set of calculations aiming to provide all the outputs to be displayed in a dedicated web site and to be used by instrument scientists, LBTO science operation team and astronomers. Finally the temporal evolution of all the atmospheric and astroclimatic parameters relevant for the LBT observations are posted in a dedicated repository that feeds the LBT Science Operation Software at Mt.Graham (see Fig.1).

The code of the automatic system is written in Fortran90, Bash and Python. Fortran is mainly used for the numerical computation[4], Bash for the management of the automatic processes and Python is used to manage the graphic analysis of the ALTA Center (see later on). We highlight that the graphic analysis has been originally developed in IDL. Later on, the code has been translated in Python to avoid the problem of licences to be replaced yearly.

Before the design phase of the automatic system the possible points of failures were analysed thoughtfully. The HPC hardware was made redundant by deploying two servers for the Meso-NH simulations. Also a backup connection was put in place for the ECMWF grib files delivery, setting up a virtual backup server on the LBTO network to be able to receive the files if INAF/Arcetri network fails. The back-up server is a virtual account on one of the LBTO servers (see Fig.1). For what concerns the servers preliminary tests on computation time permitted us to identify the architecture suitable for ALTA. The choice was the result of a trade off between

[4]Most of the hydrodynamical codes are written in Fortran90

the costs and the computing performances. The servers have been purchased and installed in the INAF/OAA CED in the first year of the contract.

3.1 ALTA Center Web Site

The development and implementation of the automatic forecast system software includes also the development of a dedicated web site conceived to host the outputs of the automatic forecast system. The URL of the ALTA Center is: *http* : *//alta.arcetri.inaf.it*. Fig.7 shows the the web-site home. Such a site has been developed at home and it is integral part of the contract. The web site has been conceived to display:

(1) Tutorial: It contains the definition of all the parameters defined and forecasted in the ALTA Center web site;

(2) Legend: it has been included to support the reader to correctly interpret the outputs displayed in the ALTA Center web site;

(3) Forecasts: the hearth of the forecast products divided in: **(3a)** forecasts of the next night and **(3b)** forecasts of the previous three nights. The forecast of the next night are those relevant for the science operation team, astronomers and instrument scientists of LBT. This link is protected by a password and freely accessible only by all members of the LBT Consortium. This is imposed by ECMWF policy as, to reduce costs, we bought initialisation data under a research contract that does not allowed the vision from third parties. Forecasts related to the previous three nights (3b) are, on the contrary, accessible by everybody. This link is very practical to appreciate by everybody the outputs provided by the automatic forecast system.

(4) Trends: the plan is to plot the trend of the forecast on a different time scales. This item has been let to be developed later on, when the system will be at a more advanced level of completeness.

(5) Climatology: computation of the climatological statistics calculated on different years. The idea is to collect with the time the outputs related to the different parameters to set-up a sort of archive that can be useful to put in evidence trends on long-time scale.

The link **Legend** includes a few fundamental concepts: the forecast timeline, the night partition and the convention for night/day phases.

3.1.1 Forecast Timeline

The link **Legend** explains us which is the forecast timeline. Model forecasts cover the whole night of observations, each night being identified by the date expressed in Mountain Standard Time (MST) when the night is starting (sun set). MST is the local time at Mt.Graham.

In Fig. 8 are shown the UT and MST time axes. Different days are identified following the UT time. Considering that in principle people could connect to the web site from different locations in the world (Tucson, Italy, Germany, US), in the following lines we report instructions to interpret correctly the model outputs with precise temporal references in order to avoid misunderstandings.

The web site permits the vision of the forecast of the night that is coming (see link *'Forecast Next Night'*) let's call that DAY J (where J is the day in Universal Time (UT)) and the forecasts of the previous night (see link *'Forecast Previous Nights'*) let's call that DAY (J-1). The simulation of the night DAY J starts at 23:00 MST of the DAY (J-1) (symbol 'diamond' on the MST axis). At 21:00 UT / 14:00 MST of DAY (J-1) (symbol 'star' on the MST axis) the forecast of the DAY J are displayed on the website through the link *'Forecast Next Night'*. At the link *'Forecast Previous Nights'* are visible the forecasts of the DAY (J-1). The simulations of DAY J done by the model cover the period starting from 00:00UT of DAY J to 15:00 UT of DAY J (or 17:00 MST of DAY (J-1) to 8:00 MST of DAY DAY J).

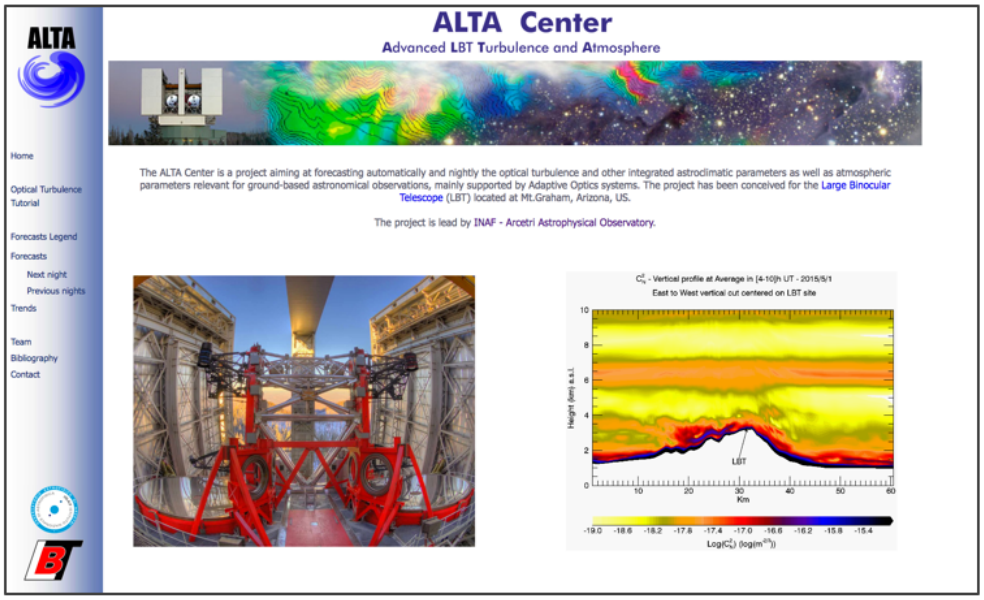

Figure 7: ALTA Center web-site home.

The displayed *'Forecasts Next Night'* covers the time frame between the sunset and the sunrise of the DAY J, which are automatically computed for the LBT site (considering position, altitude and refraction index of the atmosphere). Where possible also the times of the astronomical dawn and dusk are shown. The displayed *'Forecast Previous Nights'* cover the time frame between the sunset and the sunrise of the DAY (J-3),DAY (J-2),DAY (J-1).

At 16:00 UT / 9:00 MST of DAY (J-1) (symbol 'circle' on the MST axis) the website is updated and the forecasts related to the night that have just finished are moved to forecast of previous night (see link *'Forecast Previous Nights'*). Just after 16:00 UT / 9:00 MST of DAY (J-1) the website in the link *'Forecast Next Night'* will show a warning stating that the forecasts of the DAY J will be displayed at 21:00 UT / 14:00 MST of the DAY (J-1).

Initialisation data (i.e. forecast from the ECMWF) are calculated at 00:00UT of the DAY (J-1).

3.1.2 Night partition

For each night we provided a set of forecasts extended on the whole night. As a first baseline, we considered each night divided in three parts: the beginning, the central and the finishing part of the night. For each temporal window the state of the different parameters are displayed. For example, the average vertical profiles of all the vertical stratifications are indicated for the respective three temporal windows. Equally, it is possible to visualise the average horizontal map of the seeing (ε), isoplanatic angle (θ_0) and wavefront coherence time (τ_0) extended on a surface of 60 km $\times$ 60 km around the summit. How is the partition done ?

The whole year is defined into two macroscopic seasons:

SUMMER: [April – September]
WINTER: [October - March]

When computing time averages, the whole night time frame is divided into three parts, identifying the first, central and last part of the night. The external thresholds are the dusk and dawn. The internal time thresholds

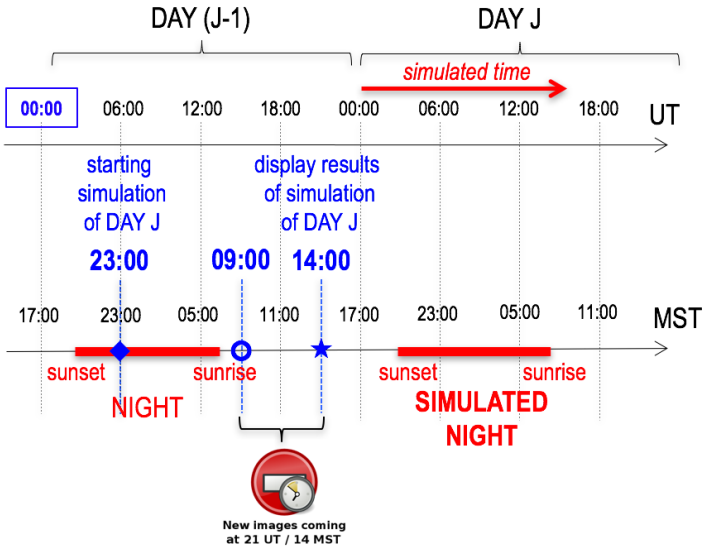

Figure 8: Forecast timeline displayed in the link *'Legend'* of ALTA Center.

depend on the current season as defined previously (see Fig. 9).

FIRST PART OF THE NIGHT: The thresholds are 06:10 UT / 23:10 MST (summer) or 05:30 UT / 22:30 MST (winter).
CENTRAL PART OF THE NIGHT: The thresholds are 06:10 UT / 23:10 MST and 8:50 UT / 01:50 MST (summer) or 05:30 UT / 22:30 MST to 09:30 UT / 02:30 MST (winter).
LAST PART OF THE NIGHT: The thresholds are 08:50 UT / 01:50 MST (summer) or 09:30 UT / 02:30 MST (winter).

3.1.3 Forecast convention for night/day phases

Each day is divided in phases by the following delimiters (see Fig. 10):

SUNRISE: The sun disk rises crossing the horizon (which is relative to the observer position) and daytime starts officially.
SUNSET: The sun disk falls crossing the horizon. Daytime ends and twilight period starts. During the twilight, ground illumination is not direct but is instead coming from the sunlight scattering in the upper atmosphere.
DUSK: The sun disk falls below 18° from the horizon. At this point there is almost no illumination coming from the sun on the lower Earth's atmosphere.
DAWN: The sun disk rises above 18° from the horizon. The lower atmosphere starts to be illuminated by scattered sunlight moving into the twilight phase.

The phase of development has been completed with the realisation of a Manual of the automatic system of ALTA that permits to our team to manage the whole system. The automatic forecast system is installed on two servers: the one dedicated to the operational activities and a back-up server useful in case of any break. A back-up of the whole automatic system has been stored on a dedicated archive. A dedicated manual has been done so that we can easily reconstruct the whole software with its procedures.

Recently the system was updated to provide a short timescale forecast (up to 4 hours in the future) computed with autoregressive techniques from both the Meso-NH model prediction and the real-time measurements

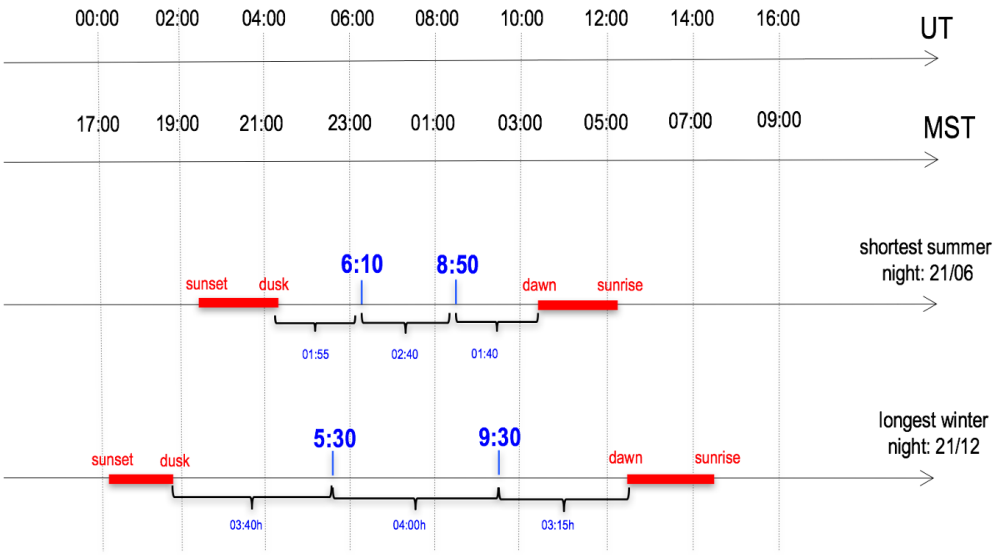

Figure 9: Night partition displayed in the link *'Legend'* of ALTA Center.

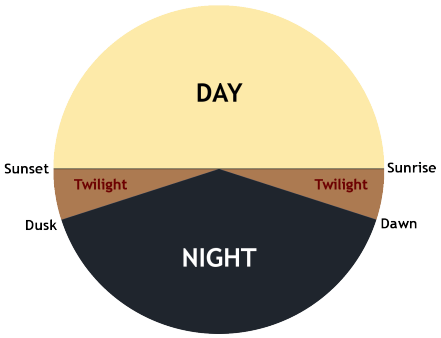

Figure 10: Graphic representation of the twilight, sunset, sunrise, dawn and dusk. Displayed in the link *'Legend'* of ALTA Center.

provided by the LBT sensors. This method greatly enhance the reliability of forecasts on the next few hours in the future and continuously update during the observing night (each hour). We will deal about that in Section 7

At the end of the first year the web-page of ALTA Center has bene completed as well as the the automatic procedure. We refer the reader to the following sections dealing about the validation of the system for atmospheric and astroclimatic parameters.

3.1.4 Forecast at short time scales

A supplementary option among the forecast products has been recently implemented on ALTA Center. Such a method, based on an autoregressive technique, implies the simultaneous use of forecasts performed previously at longer time scales and real-time measurements has been proposed by **Masciadri et al. 2020, MNRAS [6]**. This was not originally planned in the contract therefore it will be treated in Section 7. We report here the explanation of its functionality.

For those cases in which there are real-time measurements at LBT (for example sensors measuring atmospheric parameters close to the ground or DIMM measuring the seeing) ALTA Center provides, since April 2019, forecasts at different time scales. Fig.11 shows, as an example, the outcomes when it is possible to perform the forecasts at short time scales. The picture shows the temporal evolution of the parameter forecasted at 14:00 LT of the day before and extended for the whole next night obtained as explained in Fig.8 (black line), the real-time measurements that during the nights are done in situ (green line) and the forecast obtained by the model using the method proposed by [6] calculated at each full hour starting from the beginning of the night and extended for the successive four hours (red line). If the red line is not present, that means that present or previous days real-time measurements are missing.

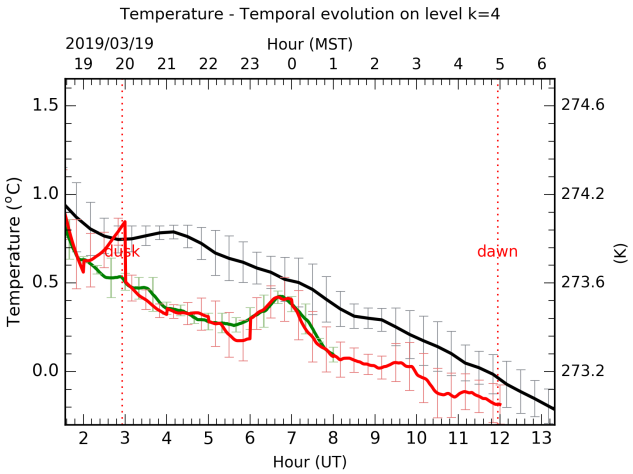

Figure 11: Example plot composed with regular forecast (black line), sensor measurements (green line) and short time scale forecast (red line), computed at 8:00 MST until 12:00 MST.

3.1.5 Forecast Products

Forecasted parameters can be selected through a curtain *Menu* (Fig.12).

Figure 12: Curtain menu permitting to the user to select the parameter and the typology of informations that he/she is looking for. Ex: horizontal map, temporal evolution during the whole night close to the surface, average vertical profile, etc.

In both cases (3a and 3b), i.e. the forecasts for the next night and for the previous three nights, ALTA Center provides:

- the temporal evolution of the atmospheric parameters at the first three model levels that correspond to the first three vertical slabs i.e. the surface layer;
- the average vertical profiles in the three partitions of each night (beginning, central and finishing part) of those parameters for which we have a vertical stratification such as the wind speed, the wind direction, the relative

humidity, the mixing ratio, ... (Ex: Fig.14, Fig.15, Fig.16, Fig.17);
- the average profiles belonging to the three partitions overlapped in the same picture to appreciate the macroscopic changes during the three major periods of the night (Ex: Fig.14, Fig.15, Fig.16, Fig.17)
- the temporal evolution of the vertical profiles all along the night of those parameters for which we have a vertical stratification (Ex: Fig.14, Fig.15, Fig.16, Fig.17)
- temporal evolution of the equivalent velocity V_{eq} - for FLAO (see Section 7)
- temporal evolution of the equivalent velocity V_{eq} - for ARGOS (see Section 7)
- temporal evolution of the equivalent velocities $V_{eq,ground}$ and $V_{eq,free}$ related to the two heights at which the two DMs are conjugated - for LINC-NIRVANA (see Section 7)
- horizontal map (2D) of the wind speed close to the surface (20 m a.g.l.) - animation related to the whole night (1h time frequency)
- horizontal map (2D) of the wind speed close to the surface (20 m a.g.l.) - average on the whole night
- horizontal map (2D) of the wind speed close to the surface (20 m a.g.l.) - average in the three partitions of each night
- horizontal map (2D) of the wind speed at 200 mb (i.e. the jet stream level) - animation related to the whole night (1h time frequency)
- horizontal map (2D) of the wind speed at 200 mb (i.e. the jet stream level) - average on the whole night (Fig.19)
- horizontal map (2D) of the wind speed at 200 mb (i.e. the jet stream level) - average in the three partitions of each night
- horizontal map (2D) of the wind speed at the height of the second DM (7.1 km) computed for a line of sight of 0, 30 and 60 degrees with respect to the zenith - for LINC-NIRVANA

- horizontal map (2D) of the $\text{seeing}_{[20m-20km]}$ - animation related to the whole night (1h time frequency)
- horizontal map (2D) of the $\text{seeing}_{[20m-600m]}$ - animation related to the whole night (1h time frequency)
- horizontal map (2D) of the $\text{seeing}_{[600m-20km]}$ - animation related to the whole night (1h time frequency)
- horizontal map (2D) of the $\text{seeing}_{[20m-20km]}$ - average on the whole night (Fig.20)
- horizontal map (2D) of the $\text{seeing}_{[20m-600m]}$ - average on the whole night
- horizontal map (2D) of the $\text{seeing}_{[600m-20km]}$ - average on the whole night
- horizontal map (2D) of the $\text{seeing}_{[20m-20km]}$ - average on the in the three partitions of each night
- horizontal map (2D) of the $\text{seeing}_{[20m-600m]}$ - average on the in the three partitions of each night
- horizontal map (2D) of the $\text{seeing}_{[600m-20km]}$ - average on the in the three partitions of each night

- horizontal map (2D) of the $\tau_{0,[20m-20km]}$ - animation related to the whole night (1h time frequency)
- horizontal map (2D) of the $\tau_{0,[20m-600m]}$ - animation related to the whole night (1h time frequency)
- horizontal map (2D) of the $\tau_{0,[600m-20km]}$ - animation related to the whole night (1h time frequency)
- horizontal map (2D) of the $\tau_{0,[20m-20km]}$ - average on the whole night (Fig.20)
- horizontal map (2D) of the $\tau_{0,[20m-600m]}$ - average on the whole night
- horizontal map (2D) of the $\tau_{0,[600m-20km]}$ - average on the whole night
- horizontal map (2D) of the $\tau_{0,[20m-20km]}$ - average on the in the three partitions of each night
- horizontal map (2D) of the $\tau_{0,[20m-600m]}$ - average on the in the three partitions of each night
- horizontal map (2D) of the $\tau_{0,[600m-20km]}$ - average on the in the three partitions of each night

- horizontal map (2D) of the $\theta_{0,[20m-20km]}$ - animation related to the whole night (1h time frequency)
- horizontal map (2D) of the $\theta_{0,[20m-20km]}$ - average on the whole night (Fig.20)
- horizontal map (2D) of the $\theta_{0,[20m-20km]}$ - average on the in the three partitions of each night

3.2 Initialisation data

Initialisation data are provided by GCMs. Different options were in principle accessible to us. We decided to use initialisation data provided by the ECMWF IFS (more precisely by the Atmospheric Model High Resolution 10-day forecast (HRES)) for three main reasons: **(1)** these are the data with the highest horizontal resolution

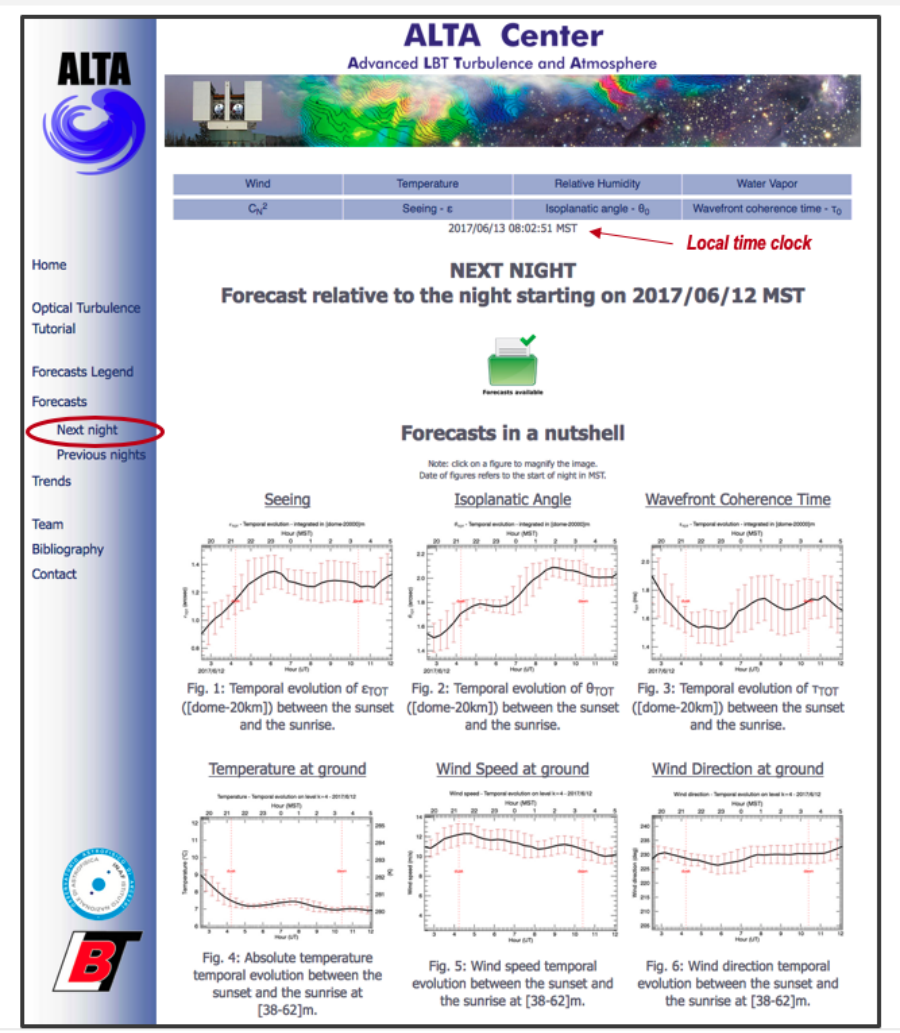

Figure 13: Screenshoot of the ALTA Center web-page displaying the forecast of the temporal evolution of the most relevant parameters for the next night.

that are available on the market therefore these are the data containing the best detailed description of the atmosphere status at large spatial scales; **(2)** these are the data that we use in general in our research studies. We are therefore very familiar with them. The mesoscale modele (Meso-Nh) that we use has been originally conceived to work with ECMWF data. The drawback is that these data are not free but this is also normal as the quality has a cost. We decided to use a *research policy* instead of a *commercial policy* as it is less expensive but this forces us of course in keeping confidential the forecasts produced by ALTA Center. In other words the possibility to access to the research policy is because our forecasts are used in application to the science operations of LBTO (astronomical research goal). This is the reason why the link of the forecasts related to the 'next night' is accessible only by the LBT consortium. Once 24H have been last, the forecast becomes a forecast of a past night and as a consequence it is accessible through the related ALTA Center link. The contract lasts one solar year, starting from March first of each year.

At the beginning of the project we used the gaussian reduced grid N640 having a horizontal resolution of [14-16] km. This was the best available at the epoch. On November 2016 we shifted to new initialisation data having a higher horizontal resolution as ECMWF released on March 2016 a new grid. We chose the octohedral gaussian reduced grid O1280 as we verified that Meso-Nh could match with this grid if some modifications in

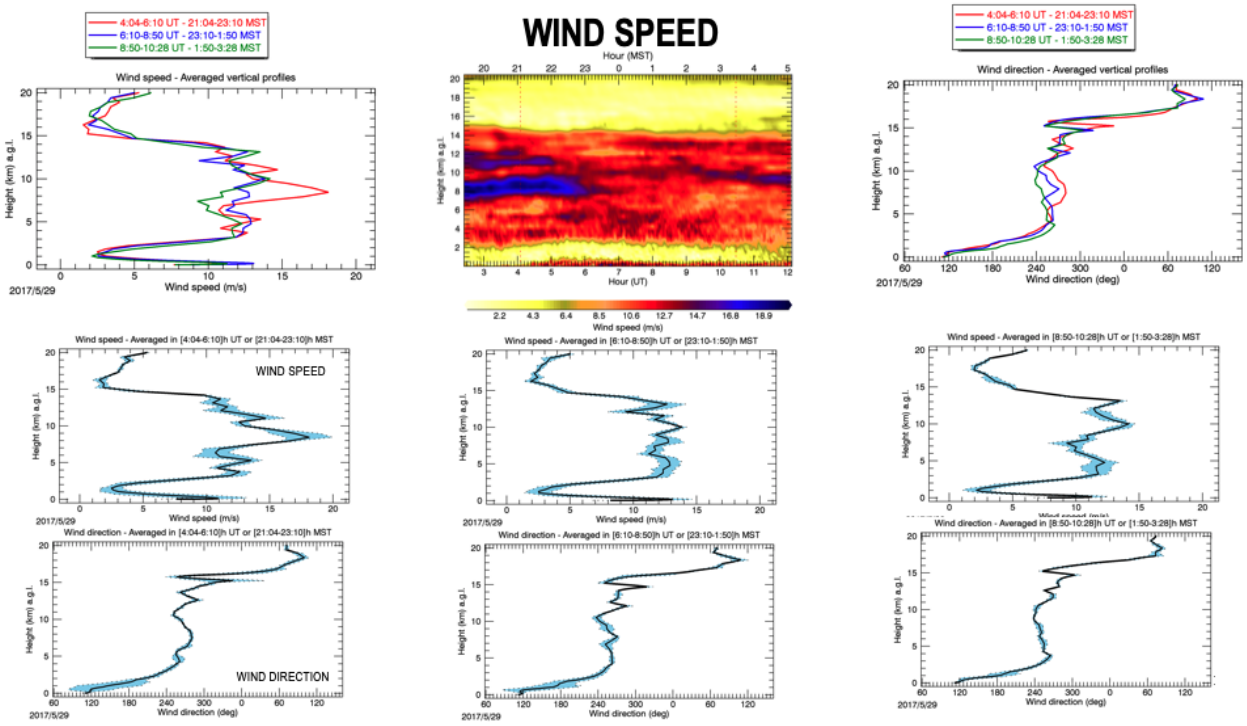

Figure 14: Composition of forecasts products related to the wind speed for one specific night. On the top-center we have the temporal evolution of the vertical distribution up to 20 km. On the top-left we have the average vertical wind speed in the three different parts of the night (see Fig. 9) to appreciate the important changes during the nights. On the top-right the same thing for the wind direction. In the second and third rows, are displayed resepctively the average wind speed and wind direction in the first (left), central (center) and last part of the night (right). The dotted lines report the $\pm\,\sigma$.

the model itself had been done. We have been encouraged in this change as we could access to these data for the same cost (without up-graded contracts) and we could maintained the gaussian reduced option. This permitted us to be sure that the impact of the initialisation data on the forecast was the same as before. All this required some work to verify that the new set-up could work properly. On February 2019, in occasion of the yearly renovation of the contract with ECMWF, we decided to change from gaussian reduced grid (O1280) to gaussian regular grid (F1280) as the procedure permitting us to use the reduced grid revealed to be very heavy. This decision forced us to perform a dedicated analysis to study the impact of different initialisation data on the ALTA Center forecasts. We could verified that the change introduced only small differences of statistical nature without any bias. This guaranteed us to change the grid assuming that the characterisation done previously with the previous grid could be preserved. Since there we are using the F1280 grid.

As recently the Meso-Nh model has been adapted to be used with initialisation data different from ECMWF, in agreement with the contractor it has been decided that it might be interesting to perform a study on sensitivity of the forecasts obtained by ALTA Center from the different initialisation data. In particular we think to those provided by the NOAA-NCAR i.e. the GFS data that are free. Such a study will be able to certainly provide a very interesting practical feedback as we will be able to better quantify the added value provided by initialisation data that are characterised by a higher resolution but are not free. It might be a way to give a value to the better quality of ECMWF data. We point out that the cost if of the order of $\sim$ K€3 for year. The cost depends on the number of initialisation data selected by the user. In case of a more complex configuration the cost might have an impact.

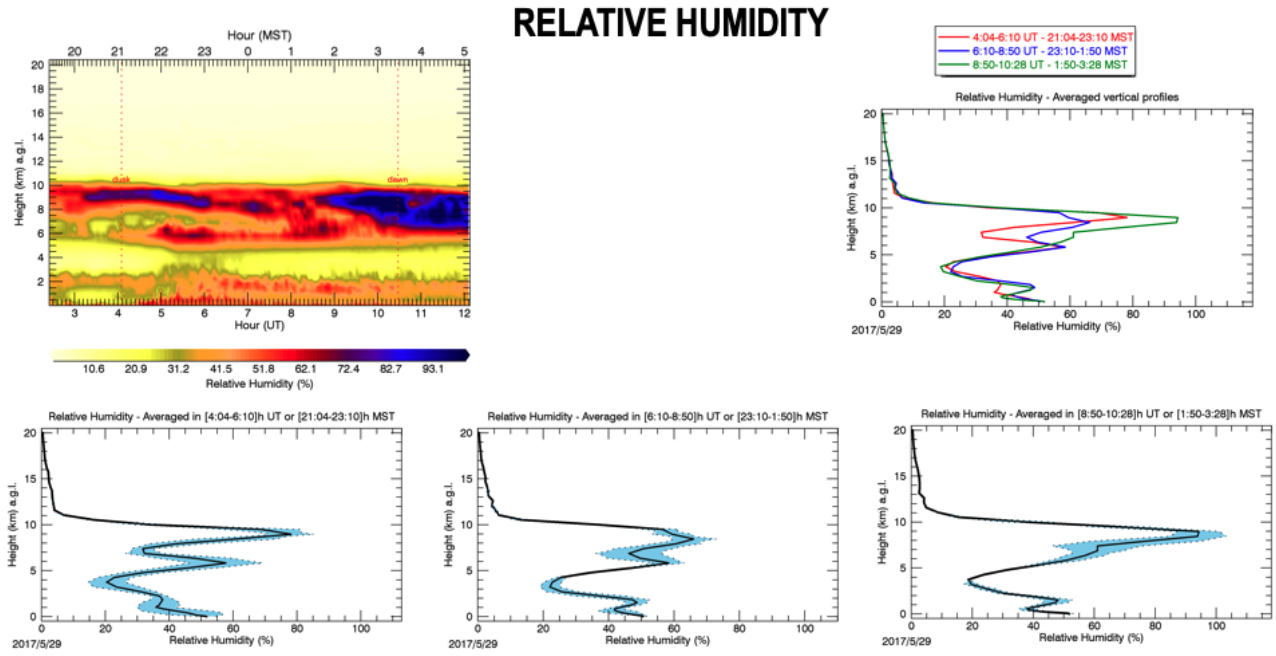

Figure 15: Top-left: temporal evolution of the vertical distribution of the relative humidity RH. Top-right: average of the vertical profile of RH in the three parts of the night. Bottom: average profile in the three parts of the night with associated σ.

3.3 Hardware

The selection of the hardware i.e. the HPC facility has been done at conclusion of a dedicate analysis aiming to find a trade-off between the cost and the architecture power. The most critical parameter for the ALTA Center application is the computational time that should be as short as possible.

The configuration of the hardware has been conceived in a way to have, for each unit (computation and storage), a back-up element. Considering that we normally assist, from one side, to a constant progress of the quality of the initialisation data (and of the GCMs that produces such a data) and of the computational technology and, on the other side, each computational facility is characterised by a typical lifetime, we agreed with the contractor that a complete refurbishment of the computational architecture would had been discussed with the contractor with a frequency of the order of 5-6 years. The purchase of new facilities is supposed to be decided taking into account **(1)** the conditions of the present architecture; **(2)** the new goals that are defined; **(3)** the potentiality of model forecast performances requested and **(4)** the cost of the architectures.

A total of around K€22 (K€11 $\times$ 2) has been invested (for the main computational facility and back-up) on a time scale of five years on 2015. We chose an architecture with a total of 128 Gb (16 modules of 8 Gb) and 4 CPU for a total of 64 cores. The cost of the storage is not relevant as we estimated around 150 Gb for year. We can add therefore K€0.5 for the storage and K€1.6 for the post-processing server that is devoted to the post-processing and to calculation of the autoregression i.e. the forecast at short time scales. A total of $\sim$ K€24 is therefore devoted to hardware. The architecture selected for ALTA Center revealed to be definitely successful with respect to our necessity both in terms of computational performances that in in terms of storing capacity. The reliability full-filled expectations and the server had no problems up to present time.

Now, at conclusion of the contract related to the first 5 years, those architecture are not any more in the market. We already tested new generation architectures that can be interesting for our application. We can anticipate that, among the different solutions available in the market, the new version of the same architecture can achieve a 40% faster computation time for $\sim$ K€16. We calculated a reduction of a factor of the order of 65

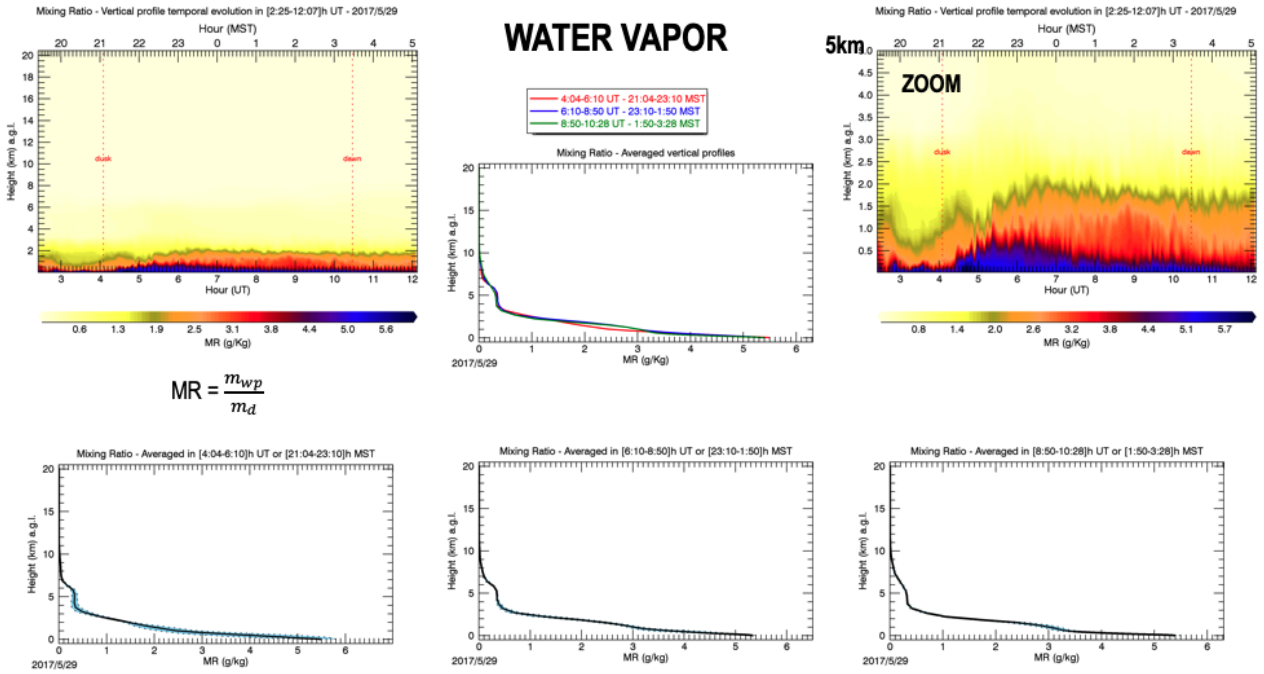

Figure 16: Top-lef: temporal evolution of the averaged vertical profile of the mixing ratio (MR). Top-right: average of the vertical distribution of the MR in the three parts of the night. Bottom: average in the three parts of the night with associated σ. The integral of the MR gives the precipitable water vapour (PWV).

% (with respect to the present time) for a different typology of architecture ($\sim$ K€22). We considered ancillary costs those relate to electric power, monitor, UPS, air conditioning.

HPC (2015)	Storage	Post-processing Server (2019)	Total
K€	K€	K€	K€
11 $\times$ 2	0.5	1.6	24

Table 1: Order of magnitude of value of the hardware related to ALTA Center at present time (2020).

3.4 Failures/breaks statistics

We report in this section some useful statistical results on the failures of the systems. We use as a reference a period of two years (January 2018 - December 2019) as a period of reference in which the system was in an complete level of development. We calculated, for this period the number of failures and the nature of failures.

(1) Failures of the ECMWF: in just 1 case, ECMWF modified the files it had already delivered after a few hours.

(2) Failures of the back-up account in Tucson: 1 case. We could not reconstruct why that account temporarily did not work. By definition this is an account very rarely used. After this specific problem we decided to implement in our system a control check that inquires regularly the account in Tucson and notifies us immediately if there is a problem even if it is not used.

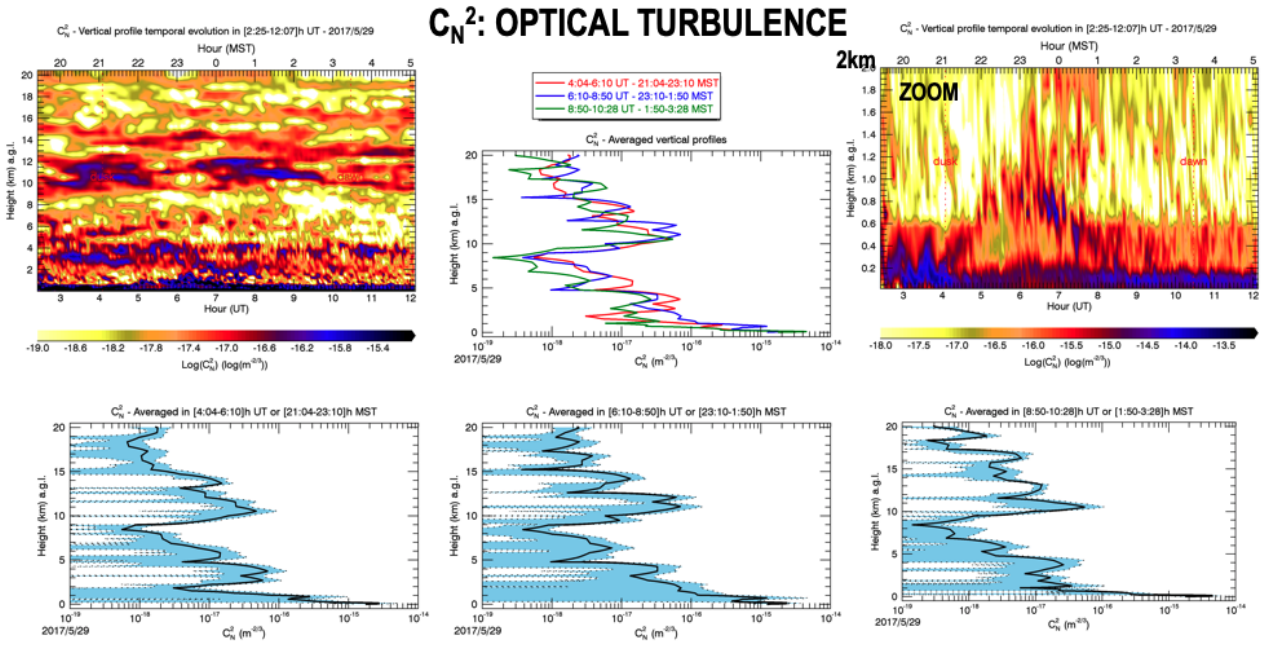

Figure 17: Top-left: temporal evolution of the C_N^2 on the 20 km. Top-right: zoom in the first 2 km. Top-center: the average vertical wind speed in the three different parts of the night. Bottom: average C_N^2 in the three parts of the night.

(3) Failures related to a too large time step: 7 cases. These are failures of the model due to the numerical instabilities. Typically this happens when the there are anomalous atmospheric conditions. These are not necessarily all lost cases. When there is a failure of whatever nature, the system send a message via e-mail to the team. In most failures of this nature, we have the time to reduce the time step and run again the simulation so to complete it within the requested interval time.

(4) Failures of local CED due to logistic (electric power problems, etc): 3 cases. In one case there was an electric power failure, in a second one a problem to the air conditioning system that was stuck because to a problem to the fan. The last case was related to a network problem. The web-page was not available. After the problem we had with the air-conditioning the CED in Arcetri has been up-graded. The fan has been replaced and a thermometer has been installed to control the indoor temperature. Since there we had not problems of this nature.

Thanks to the system of warnings that we implemented in ALTA Center system, we can say that we had only two cases in which the simulation/information was lost on a period of two years. In the other cases (very few in any cases) we could solve in real-time the problem. We recently decided to get lighter the procedure storing in a log file the failure problems using a set of predefined flags.

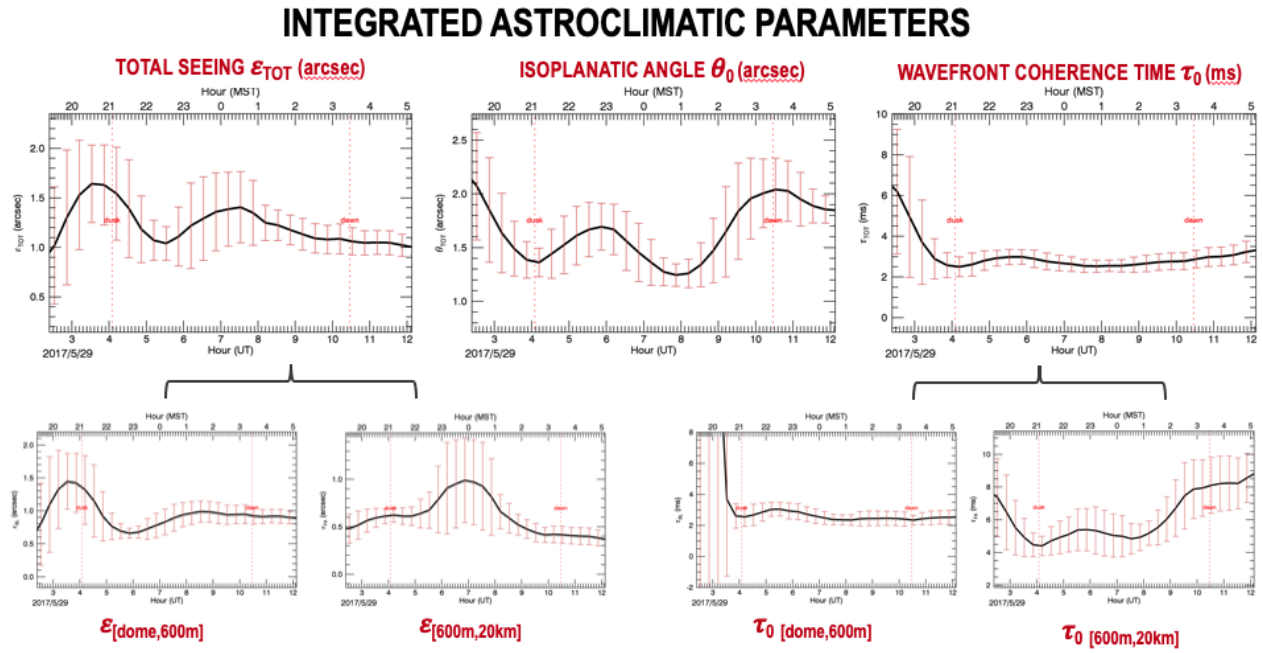

Figure 18: Temporal evolution of the most relevant astroclimatic parameters: the seeing (top-left), the isoplanatic angle θ_0 (top center) and the wavefront coherence time τ_0 (top right). On the bottom are shown the seeing and the τ_0 in the boundary layer and the free atmosphere.

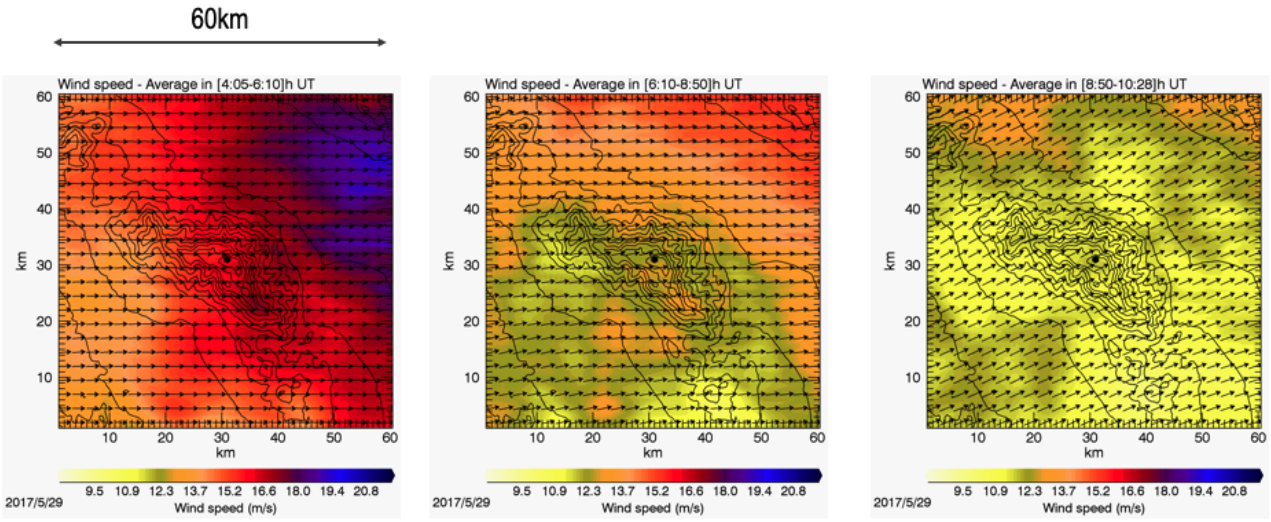

Figure 19: 2D map extended on 60 km $'\times$ 60 km of the WS at 200 mb. The three panels shows the average in the three parts of the night (see Fig.9).

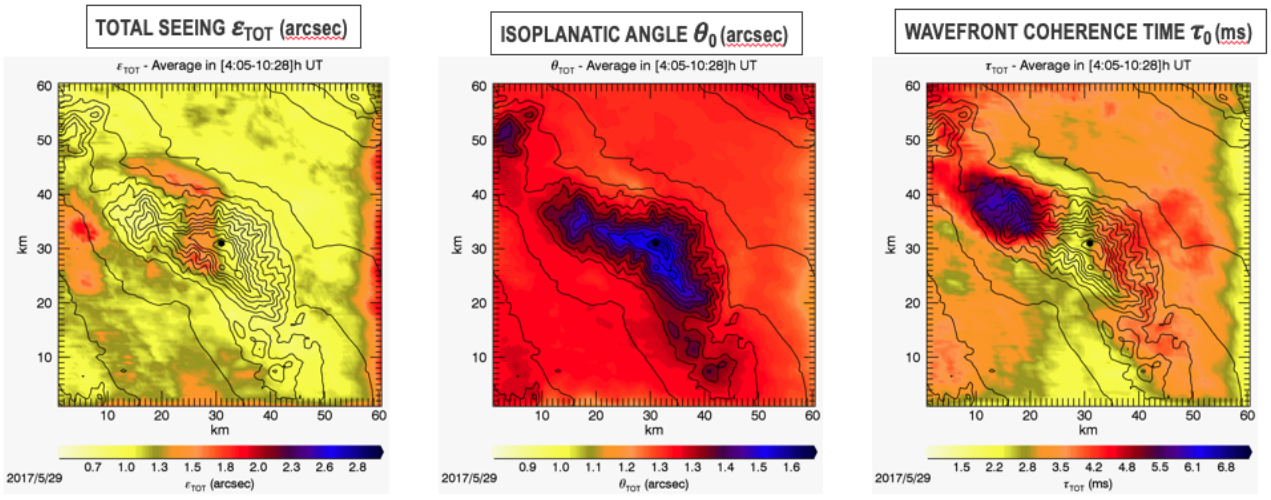

Figure 20: 2D map extended on 60 km ′× 60 km of the seeing (ε), isoplanatic angle (θ_0) and wavefront coherence time (τ_0). The three panels shows the average in the three parts of the night (see Fig.9).

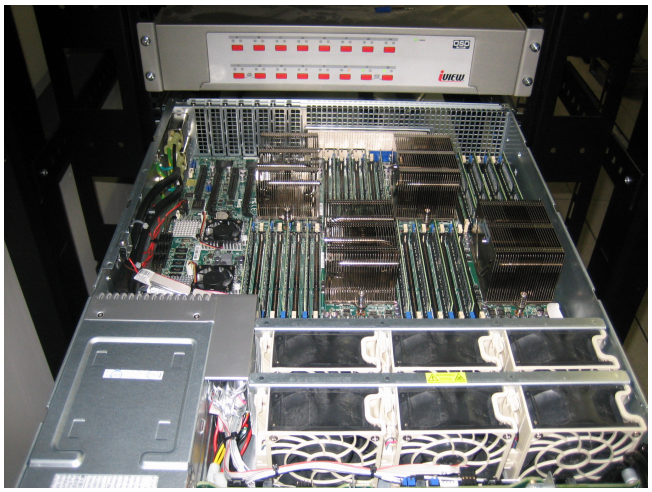

Figure 21: Internal vision of a module of the ALTA Center HPC facility.

4 Milestone 2: Development and deployment of the atmospheric parameters prediction with corresponding data access capabilities from LBTO

The second year of activity has been devoted to the validation of the operational forecast of the atmospherical parameters. All the atmospheric parameters can be forecasted with the Meso-Nh model that does not require any calibration at priori. The study consisted therefore on:

(1) Defining the geometrical configuration of the model;

(2) Retrieving from the LBTO telemetry the real-time measurements of a predefined rich statistical sample of nights to be used as a reference for the model validation. We identified a rich sample of nights uniformly distributed along a solar year so to avoid any bias of whatever nature;

(3) Performing simulations related to all the nights belonging to the selected sample and quantifying the model performances in forecasting the different selected parameters above Mt.Graham. Two different approaches have been used to quantify the model performances: (A) the calculation of the classical statistical operators BIAS, root mean square error RMSE and standard deviation σ and (B) the calculation of contingency table with annexed statistical operators i.e. the percentage of corrected detection PC, the probability of detection of a specific parameter in a specific interval of values POD_i, the probability of extremely bad detection EBD.

Results of this activity is described in the paper **Turchi et al. 2017, MNRAS**, [7] (see Section 8). It contains the description of the model configuration selected for ALTA and a complete validation of the model for the following atmospherical parameters close to the ground:

- temperature (T) @ 58 m above the ground level (a.g.l.),
- relative humidity (RH) @ 58 m a.g.l.,
- wind speed (WS) @ 56 m a.g.l.,
- wind direction (WD) @ 56 m a.g.l.
- precipitable water vapour (PWV)[5] integrating the water vapour on the whole column above the LBT

The height above the ground depends on the position of the sensors located on the top of the LBT dome Fig.22. The model validation has been performed on a rich statistical sample of nights (144 nights) distributed uniformly along two solar years (2014 and 2015). The peer-reviewed paper has been published on 2017 but ALTA started to deliver operational forecasts of these parameters since the end of 2016 i.e. since T_0+12. Obviously the analysis and the model validation has been performed on dates belonging to the past.

As defined in the MoU of ALTA Center at T_0+18 ALTA Center started to deliver forecasts all the atmospherical parameters that we have just cited through the ALTA Center web-page. The peer-reviewed paper was completed, submitted and published on 2017. Preliminary results have been presented at the SPIE of 2016 in Edimburgh ([9]) joint with a paper addressed to the employment of ALTA Center in the LBTO operations leaded by the LBTO director, Christian Veillet ([1]).

We refer the readers to the Turchi et al. paper [7] for detailed results and discussions annexed. We summarise here the main conclusions in terms of RMSE and σ and in terms of probability of detection (POD_i), percent of correct detection (PC) and extremely bad detection (EBD).

Fig.23 and Fig.24 show the scattering plot for the temperature and the relative humidity. Fig.25 shows the scattering plot for the WS obtained with a maximum resolution of 500 m and of 100 m. Fig.26 shows the scattering plot for the WD obtained filtering out values having WS $\leq$ to 3ms-1, 5ms-1 and 10ms-1. Fig.27,

[5]The PWV was not originally included among the deliverables.

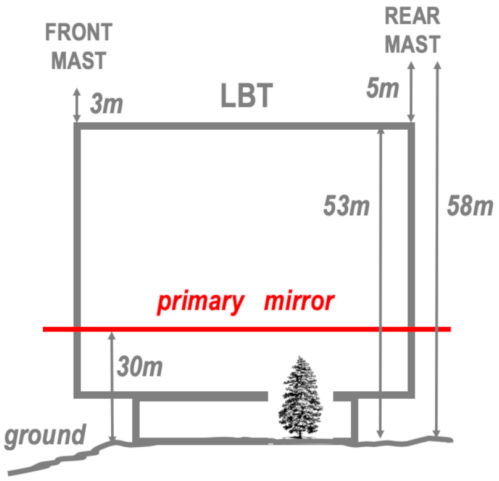

Figure 22: Positions of the two weather masts on the top of the LBT dome.

Fig.28, Fig.29 and Fig.30 show the contingency tables related to temperature, RH, WS and WD with associated POD_i, PC and EBD. Fig.31 reports the same parameters related to the WD but associated to samples filtered out from values with a WS $\leq$ 3ms^{-1}, 5ms^{-1} and 10 ms^{-1}.

Conclusions are:

(i) The model has an excellent degree of reliability in reconstructing the **temperature**, with bias, RMSE and σ below 1°C. We obtained an excellent PC = 91.7 % and all POD_i are between 84 and 99 %.

(ii) The model shows good performances in reconstructing the **relative humidity**. We find a very satisfactory bias = -2.36 %, RMSE is around 14 % and σ = 13.8 %. Besides, PC = 71.8 % is good too. The most critical POD_i for the RH is POD3, which is the probability of detecting a RH larger than the second tertile. We obtained POD3 = 61%. The model correctly discriminates the weak and the strong values of RH. We would like to improve the dispersion of the very high values of RH but the present result is already more than satisfactory.

(iii) The model shows good performance in reconstructing the **wind speed** with an RMSE ranging from 2.4 to 2.7 ms^{-1} , depending on the horizontal resolution (500 or 100 m). We observed that the resolution of 100 m is necessary only when the wind speed is large ($\geq$ 8.5 ms^{-1}) otherwise 500 m can provide even better results. We conceived, therefore, a hybrid treatment that considers the model outputs from the run having the highest resolution of 500 m when the average of the wind speed of the night is below 8.5 ms^{-1} and a resolution of 100 m when it is larger than 8.5 ms^{-1}. With such a hybrid configuration, we obtained a very satisfactory PC of the order of 65 %, POD1 = 65.7 %, POD2 = 45 % and POD3 = 84.8 %. We highlight that POD3 is the most important result for observational applications because it refers to the strong wind case that is the most critical one for telescope operations. We conclude that model performance is excellent in this respect.

(iv) Also the results obtained for the **wind direction** are very satisfactory, with an $RMSE_{rel}$ = 16.9 % if we consider all data with wind speeds greater than 3 ms^{-1}. Besides, we observed that $RMSE_{rel}$ can reach 8.8 % if we consider all data with a wind speed larger than 10 ms^{-1}. This means that the higher the wind speed, the better is the reconstruction of the wind direction by the model. Values of PC and POD_i improve also on passing from a filtering of 3 to 10 ms^{-1} with the best PC = 80.5 %. POD_i in all four quadrants is excellent with values always larger than 72 % and, when we filter out wind speeds lower than 10 ms^{-1} , model performance achieves percentages larger than 90 % (see Fig.31). In particular, POD_{SW}, related to the most

interesting quadrant from which the wind comes from more frequently (south-west), is an excellent 85.5 %.

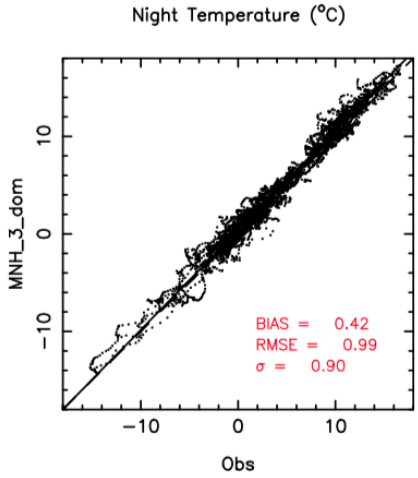

Figure 23: *Extracted from Turchi et al. 2017 ([7]) - Fig.6*: Scatter plot for temperature, comparing model outputs (MNH) and measurements (Obs). The full black line is the regression line passing by the origin, while the dashed line represents the reference diagonal line for unbiased results.

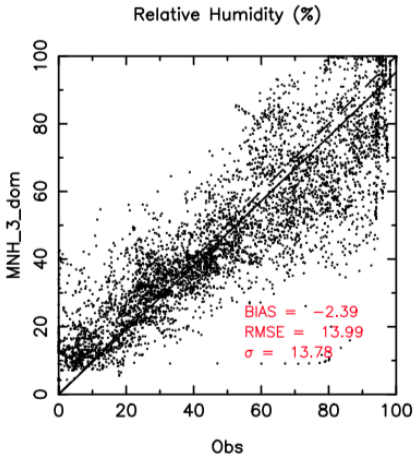

Figure 24: *Extracted from Turchi et al. 2017 ([7]) - Fig.7*: Scatter plot for RH, comparing model outputs (MNH) and measurements (Obs). The full black line is the regression line passing by the origin, while the dashed line represents the reference diagonal line for un- biased results.

More recently ALTA Center has been equipped with a supplementary method that provides forecasts at short time scales i.e. a few hours from the present time. The method is based on an autoregressive technique and it is presented in Section 7. As expected, model performances achieve much better scores in this configuration. We refer the reader to Section 7 for more details. We only mention here that the method has been validated on LBTO data and results published on a peer-reviewed paper. The method has been implemented in the operational ALTA Center system and it is currently running nightly.

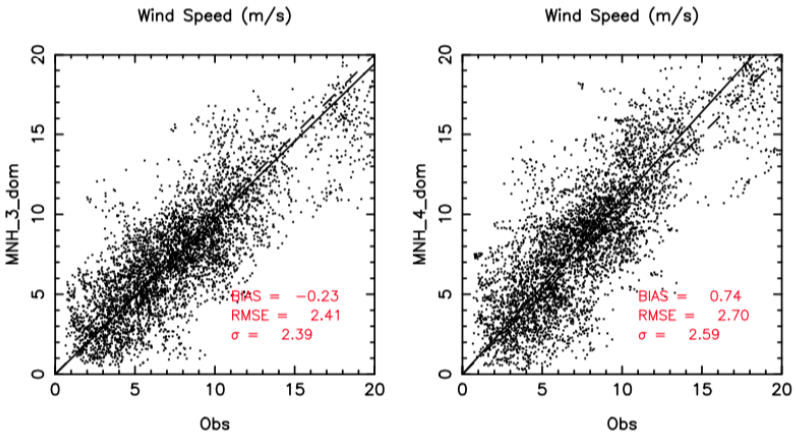

Figure 25: *Extracted from Turchi et al. 2017 ([7]) - Fig.10*: Scatter plot for wind speed, comparing model outputs (MNH) and measurements (Obs). The full black line is the regression line passing by the origin, while the dashed line represents the reference diagonal line for unbiased results. Left: Results obtained with the model output at 500-m horizontal resolution (domain 3). Right: Results obtained with the model output at 100-m horizontal resolution (domain 4).

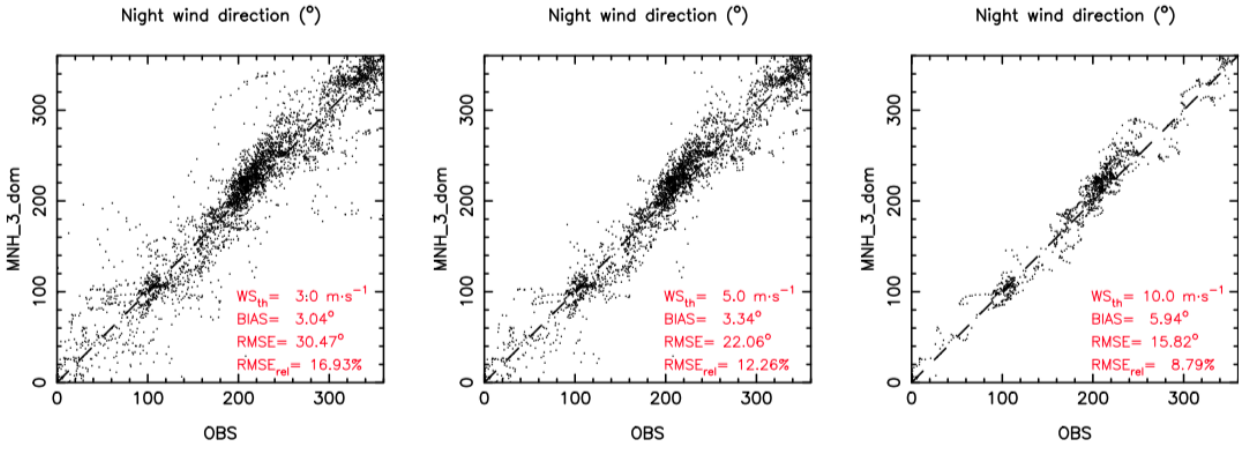

Figure 26: *Extracted from Turchi et al. 2017 - Fig.11*: Scatter plots for wind direction, comparing model outputs (MNH) and measurements (OBS). The dashed line represents the reference diagonal line for unbiased results. Wind directions are filtered by the corresponding value of the wind speed. Left: Minimum wind speed of 3 ms^{-1}. Centre: Minimum wind speed of 5 ms^{-1}. Right: Minimum wind speed of 10 ms^{-1}.

In Section 4.2 we deal about a few items that complement topics that have been treated in the peer-reviewed paper and that are relevant to complete the information.

4.1 Precipitable water vapour: PWV

The precipitable water vapour deserves a dedicated section. Even if the relative humidity RH was included since the original plan of the contract in the set of atmospheric parameters to be forecasted by ALTA and even of this parameter provides information on the water vapour content in the atmosphere, LBTO expressed since the beginning of 2016 the necessity to include in the set of parameters the to be forecasted also the PWV, an

Table 6. 3 × 3 contingency table for the absolute temperature during the night, at 55.5 m a.g.l. at LBT, for the sample of 144 nights. We use the Meso-Nh $\Delta X = 500$ m configuration.

Temperature (°C)		Observations		
		$T < 0.7$	$0.7 < T < 7.6$	$T > 7.6$
Model	$T < 0.7$	1381	79	0
	$0.7 < T < 7.6$	267	1841	20
	$T > 7.6$	0	67	1546

Sample size: 5201; PC: 91.7 per cent; EBD: 0.0 per cent; POD_1: 83.8 per cent; POD_2: 92.7 per cent; POD_3: 98.7 per cent.

Figure 27: Extracted from Turchi et al. 2017 ([7]) - Table 6

Table 7. 3 × 3 contingency table for the RH during the night, at 55.5 m a.g.l. at LBT, for the sample of 143 nights. We use the Meso-Nh $\Delta X = 500$ m configuration.

Relative humidity (%)		Observations		
		RH < 30.6	30.6 < RH < 67.4	RH > 67.4
Model	RH < 30.6	1199	183	14
	30.6 < RH < 67.4	412	1475	649
	RH > 67.4	0	196	1037

Sample size: 5165; PC: 71.8 per cent; EBD: 0.3 per cent; POD_1: 74.4 per cent; POD_2: 79.6 per cent; POD_3: 61.0 per cent.

Figure 28: *Extracted from Turchi et al. 2017 ([7]) - Table 7*

extremely critical parameter for the observation done with the LBTI. This parameter provides us information on the water vapour content on the whole atmosphere.

The PWV (mm) is the total atmospheric water vapour contained in a vertical column of unit cross-sectional area extending between any two specified levels. It is commonly expressed in terms of the height to which that water substance would stand if completely condensed and collected in a vessel of the same unit cross section. The total precipitable water is that contained in a column of unit cross section extending all of the way from the earth's surface to the top of the atmosphere. The precipitable water vapour (PWV) is given by:

$$PWV = \frac{10^3}{\rho g} \int_{p_{sup}}^{p_{inf}} MR dp \tag{1}$$

where MR is the mixing ration of the water vapour in (kg/kg), p is the atmospheric pressure in (Pa), p_{inf} is the pressure at 20m a.g.l., p_{sup} is the pressure at 20km a.g.l., ρ is the water density in (kg/m^3), g is the standard gravity in (m/s^2) and PWV is in (mm). To retrieve the PWV we need therefore the MR all along the atmosphere i.e. the mixing ration stratification.

Unfortunately observations of the water vapour observations taken nightly by the Submillimeter Telescope (SMT) located on the summit of Mt.Graham, close to LBT do not provide the mixing ratio as a function of the height i.e. MR(h) but just the water vapour partial pressure at ground:

Table 8. 3 × 3 contingency table for the wind speed during the night, at 58 m a.g.l. at LBT, for the sample of 139 nights. We use the Meso-Nh $\Delta X = 500$ m configuration.

Wind speed (m s^{-1}) 500-m resolution		Observations WS < 4.9	4.9 < WS < 8.5	WS > 8.5
Model	WS < 4.9	847	388	24
	4.9 < WS < 8.5	368	1036	515
	WS > 8.5	46	365	1407

Sample size: 4996; PC: 65.9 per cent; EBD: 1.4 per cent; POD_1: 67.2 per cent; POD_2: 57.9 per cent; POD_3: 72.3 per cent.

Figure 29: *Extracted from Turchi et al. 2017 ([7]) - Table 8*

Table 10. 4 × 4 contingency table for the wind direction during the night, at 58 m a.g.l. at LBT. We use the Meso-Nh $\Delta X = 500$ m configuration. Wind speed (WS) threshold is 3 m s^{-1}.

Wind direction WS > 3 m s^{-1}		Observations North	East	South	West
Model	North	737	53	20	145
	East	63	517	125	5
	South	21	63	1177	74
	West	85	1	434	903

Sample size: 4423; PC: 75.4 per cent; EBD: 1.1 per cent; POD_N: 81.3 per cent; POD_E: 81.5 per cent; POD_S: 67.0 per cent; POD_W: 80.1 per cent.

Figure 30: *Extracted from Turchi et al. 2017 ([7])- Table 10*

$$e = e^{sat}\frac{RH}{100}(hPa) \tag{2}$$

where e_{sat} is the water vapour pressure at saturation conditions. These measurements are therefore not suitable to retrieve the PWV. To validate the model we decided for a different solution. We validated the model on a different astronomical site (Cerro Paranal in Chile), the site of the Very Large Telescope (VLT) by using measurements of the PWV performed with a radiometer that is nightly running in situ. This permitted us to validate the automatic forecast system that we implemented in ALTA Center for both the MR(h) and the PWV i.e. for both the vertical stratification and the integral portion of water vapour. This validation has been performed on a rich statistical sample of nights uniformly distributed along two solar years (120 nights in 2013 and 120 nights in 2017[6]). We therefore compared forecasts provided by the model and by observations on around 240 nights. We quantified the model performances using the classical statistical operators (bias, RMSE, σ) as well as the probability of detection POD_i, percentage of corrected detection PC and extremely bad detection EBD retrieved from the contingency tables.

Once verified the good performances obtained by the model we then applied the same algorithm to the ALTA Center system and we compared, in statistical terms, the model performances with what obtained in the literature at Mt.Graham using measurements coming from the GOES satellites ([10]) that are obviously not in

[6]The analysis performed in two different years has been done to verify the stability on long time scales

Table 11. Contingency table statistical indicators for the wind direction during the night computed with different wind speed filters, at 58 m a.g.l. at LBT. We use the Meso-Nh $\Delta X = 500$ m configuration.

Operator	Wind speed filters		
	WS > 3 m s^{-1}(%)	WS > 5 m s^{-1}(%)	WS > 10 m s^{-1}(%)
PC	75.4	78.7	80.5
EBD	1.1	0.1	0.0
POD_N	81.3	85.8	85.5
POD_E	81.5	89.2	97.5
POD_S	67.0	68.0	71.8
POD_W	80.1	85.1	87.7

Figure 31: *Extracted from Turchi et al. 2017 ([7]) - Table 11*

Table 10. Comparison between the values (first quartile, median, and third quartile) as obtained by the MNH model (from ALTA Center project) on one solar year and the values as retrieved by Carrasco et al. (2017) on a sample of 58 months between 1993 and 1999. See the text for more details.

	First quartile (mm)	Median (mm)	Third quartile (mm)
ALTA	1.9	2.9	4.1
Carrasco et. al (2017)	2.0	2.9	4.3

Figure 32: Model performances in reconstructing the PWV by comparison with climatological estimates provided by GEOS satellites images. Extracted from Turchi et al. 2019 ([11]).

situ measurements. We performed therefore estimates in climatological terms. This means that we could show that the median values as well as the first and third quartiles are well reconstructed by our model (see Fig.32).

Results of our analysis have been published on the paper **Turchi et al. 2019, MNRAS** [11]. For more details we refer the reader to this paper. Fig.33 shows the cumulative distribution and the histogram of the PWV calculated on a sample of 283 distributed on one solar year between 2016/09/21 and 2017/09/21.

In the same paper we could prove that a mesoscale model such as the one used by the ALTA Center is able to provide more accurate estimates of the PWV with respect to what can be retrieved by General Circulation Models (GCMs). The latter are model extended on the whole Earth and are commonly used for weather forecasts. They are obviously characterised by lower horizontal resolution than the mesoscale models. The GCM of the European Centre for Medium Range Weather Forecasts have a horizontal resolution of around 9 km. **In the same paper [11] we could prove that the RMSE between the PWV forecasts by the Meso-Nh model and observations are smaller than a factor 2 with respect to the RMSE between the PWV forecasts by the ECMWF and observations.** This concretely justifies the use of such a kind of typology of models to support the LBT and LBTI operations.

In conclusion we can affirm that ALTA Center is therefore able today to provide vertical stratification of the MR(h) as well as PWV with performances that reproduce the climatological distribution observed in situ.

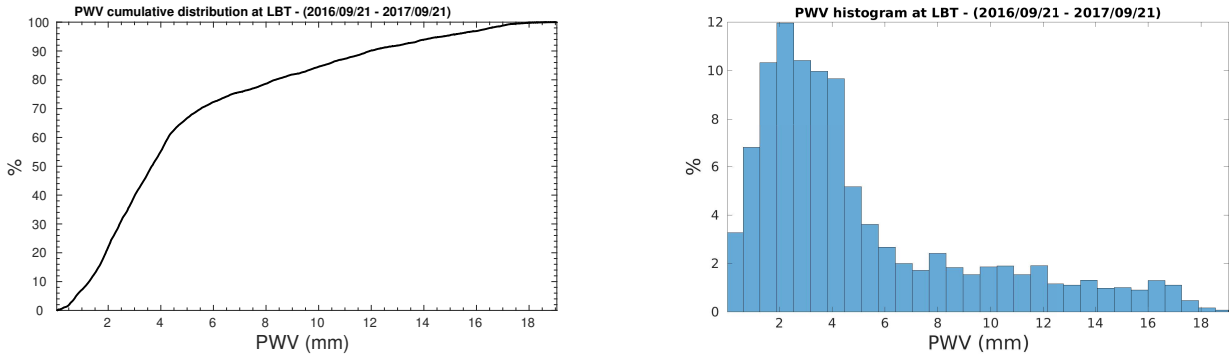

Figure 33: Cumulative distribution (left) and histogram (right) of PWV values on Mount Graham forecasted by MNH models provided by the ALTA Center. Data refer to 283 nights between 2016/09/21 and 2017/09/21. Extracted from Turchi et al. 2019 ([11]).

A few words on the radiometer used for the model validation. It is called LHATPRO, it has been validated by ESO against radiosoundings [12] showing an accuracy of 0.1 mm and a precision of 0.03 mm. Since a few years it runs routinely at Cerro Paranal (VLT). This instrument is completely automated and is manufactured by Radiometer Physics GmbH. It uses multiple microwave channels in the frequency bands of 183 GHz (H2O) and 51–58 GHz (O2) in order to retrieve, among others, the humidity and temperature profiles up to 10 km of altitude above the ground level. Measurements are taken on 39 vertical levels with a resolution that varies from 10 m at the ground level up to 1 km at the topmost height. It might be useful to implement a similar instrument on the Mt.Graham summit. Not really for the validation but for the application of the method of the autoregression (see Section 7) for which real-time measurements are necessary. Said that the order of magnitude of the cost of such an instrument is 100 Keuro. LBTO is actually elaborating a program at long time scale aiming to equip the Observatory with further instrumentation necessary to support LBTO operations. LHATPRO has been inserted in list of suitable instruments but the priority will be established taking into account the general panorama and by making a trade-off between scientific interests and costs.

4.2 Wind speed and direction estimate

As it is extensively described in the paper Turchi et al. 2017, the sensors monitoring the atmospheric parameters are located on the top of the LBT dome. There are two sensors placed on two masts located on the top of the LBT dome in front and rear with respect to the dome as shown in Fig.34. In the Turchi et al. paper it has been observed that, when wind speed blows in front to the telescope dome, the rear sensors measurement can be affected and the measurements is not reliable (Fig.35). In the paper it has been proposed a strategy to select the WS from the front or rear sensors depending on the wind direction. Of course the telescope rotates during the night as it has to observe along different lines of sights. That means that at each instant we have to identify which sensor to consider on for the WS. By looking at the minimum RMSE on a rich statistical sample of nights, it has been concluded to consider the front sensor if the wind direction blows in the $\pm 30°$ with the respect to the incoming wind direction, the rear sensor otherwise (Fig.36). This solution provides a satisfactory results in statistical terms as shown in Fig.37. The RMSE of the scattering plot between observations and forecasts is comparable to what obtained at Cerro Paranal where the sensors selection are not dependent from the wind direction as they are located in a fixed position independent from the telescope rotation.

If we can consider ourselves satisfied from a statistical point of view, more recently we observe that, looking at individual nights, the problem has not completely disappeared. Looking at Fig.38 indeed, related to one specific night, it is possible to observe that, even if the wind blows at around 90° with respect to line of sight, the WS from the front sensor (yellow line) is definitely much better correlated to the WS forecasted from the model (black line) with respect to the rear one (green line). That means that the model forecast is probably well reconstructed but if we take as a reference the rear obs. wind we conclude that the model did a great

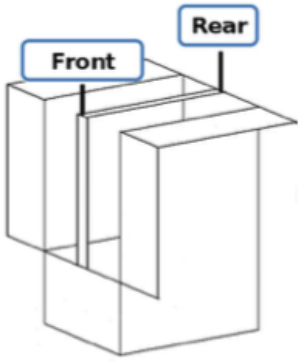

Figure 34: *Extracted from Turchi et al. 2017 ([7]) - Fig.1*

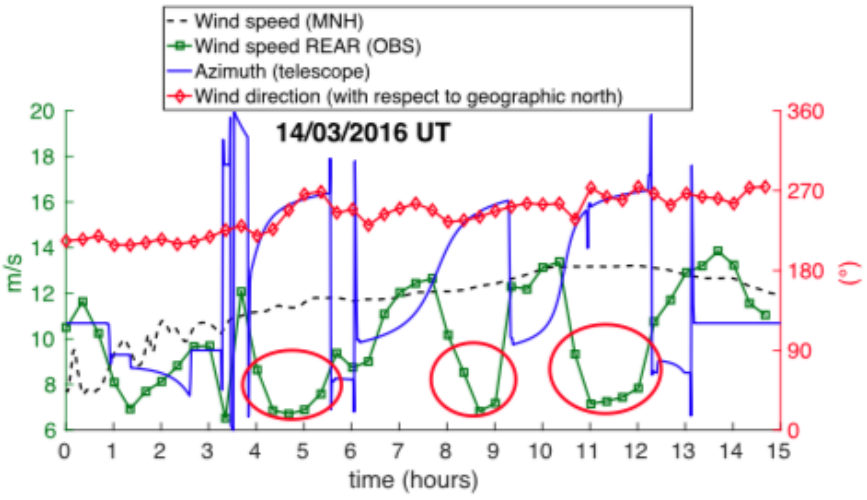

Figure 35: *Extracted from Turchi et al. 2017 ([7]) - Fig.8*

mistake while the right reference in this case is highly probably the front sensor (and not the rear as the strategy developed in Turchi et al. 2017 says). This does not mean that the strategy developed by Turchi et al. 2017 is wrong but simply that this stratgey takes into account things in statistical terms and sometimes, from an individual point of view, we can have cases (as those shown in Fig.38) in which the good reference to be taken into account can be different with respect to what described by this strategy. This is particularly important from the point of view of the forecast on individual nights, even more important for the application to the forecast at short time scale where the forecast depends also on the real-time measurements (see Section 7). A similar situation can be observed on a different night (see Fig.39). The solution of this problem is not obvious. Also the argument to consider as the right reference the closest wind speed to the model prediction has obviously its own bias. Ideally the best solution should take an independent identification of the right observed WS.
At present this problem has not yet been solved. We proposed however a practice that might help in eliminating some possible causes. We propose indeed to add a back-up sensors to be placed besides the existent rear/front sensors. This solution can permit us to be sure that there are no intrinsic software or hardware problems in the sensors. Of course the possibility to have sensors that are independet from the rotation dome should be perfect

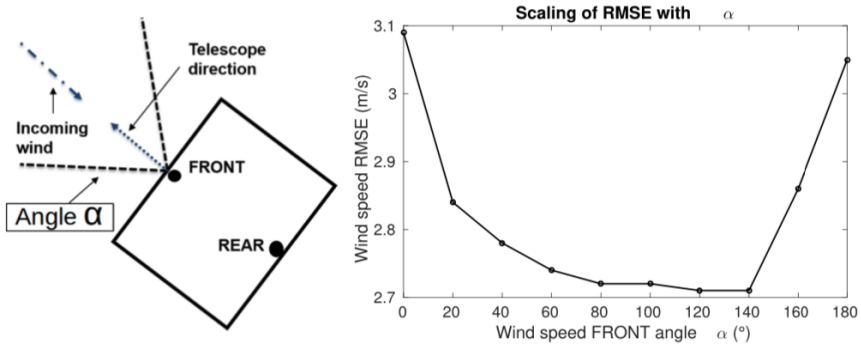

Figure 36: *Extracted from Turchi et al. 2017 - Fig.9*

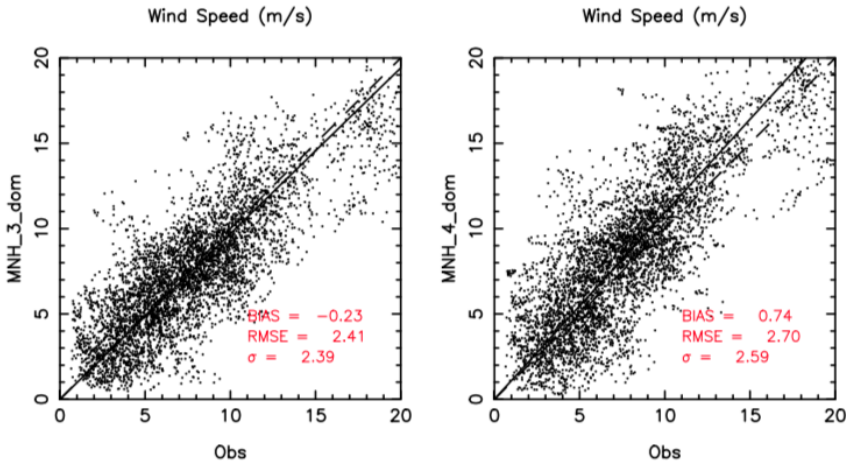

Figure 37: *Extracted from Turchi et al. 2017 - Fig.10* Scattering plot of the observed and forecasted wind speed close to the ground obtained with a configuration of 3 and 4 domains.

but not realistic.

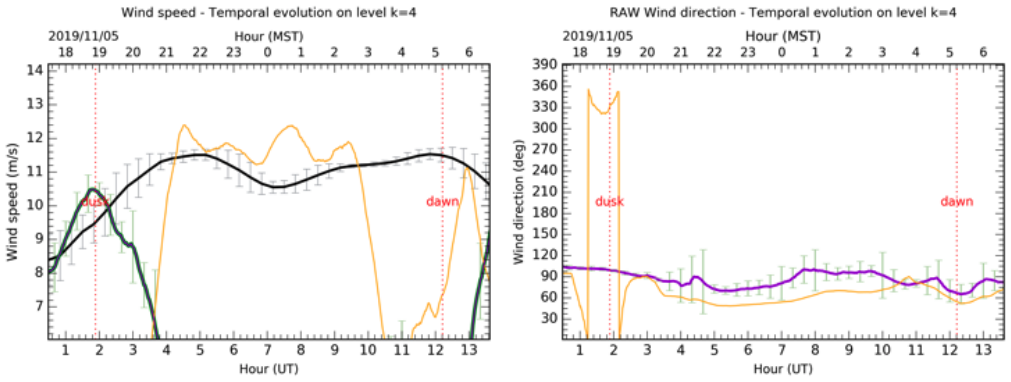

Figure 38: **Black line - model:** WS forecast at long time scale; **Yellow line - obs.:** WS front sensor; **Violet line - obs.:** WS rear sensor; **Green line - obs.:** composite (rear-front) following strategy described in Turchi et al. 2017.

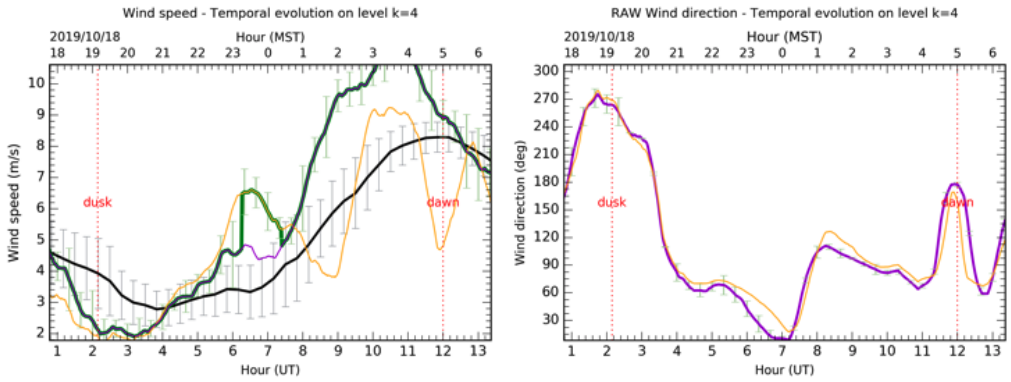

Figure 39: **Black line - model:** WS forecast at long time scale; **Yellow line - obs.:** WS front sensor; **Violet line - obs.:** WS rear sensor; **Green line - obs.:** composite (rear-front) following strategy described in Turchi et al. 2017.